Upsilons in $\sqrt{s_{NN}} = 193$ GeV U+U collisions

STAR analysis note

PA:
Róbert Vértesi
vertesi.robert@wigner.mta.hu

Institute of the ASCR, Prague/Řež

Wigner RCP, Budapest

Budapest, August 3, 2015

Abstract

Analysis of year 2012 $\sqrt{s_{NN}} = 193$ GeV U+U data was done in a similar way to Υ measurements in Au+Au collisions at $\sqrt{s_{NN}} = 200$ GeV, recently published in Ref. [1] and detailed in the corresponding analysis note [2]. The main results are the Υ(1S+2S+3S) and Υ(1S) production cross-section $B_{\rm ee}({\rm d}\sigma_\Upsilon/{\rm d}y)$, the spectra $B_{\rm ee}({\rm d}\sigma^2_\Upsilon/{\rm d}y{\rm d}p_{\rm T})$, and the nuclear modification factor versus centrality $R_{\rm AA}(N_{\rm part})$. The excited states Υ(2S+3S) seem to be present but not significantly. These are also shown.

Contents

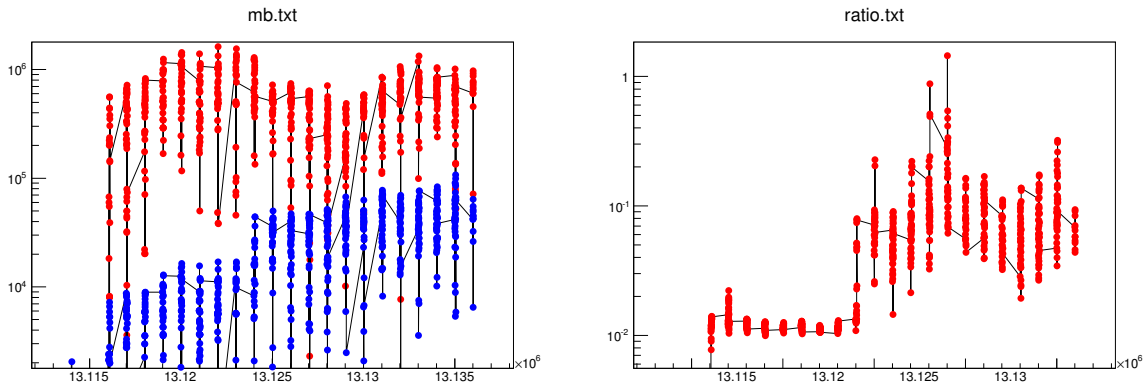

Figure 1: *Left:* Number of Minbias (red) vs. NPE18 (blue) events by run number; *right:* Ratio of NPE18 to Minbias evens by run number.

1 Reconstruction of the Υ

The $\Upsilon \to e^- e^+$ decay channel, with a branching ratio $B_{ee} \approx 2.4$ %, was studied. Analysis of year 2012 $\sqrt{s_{NN}} = 193$ GeV U+U data was done in a similar way to recently published Υ measurements in p+p, d+Au and Au+Au collisions at $\sqrt{s_{NN}} = 200$ GeV [1, 2].

1.1 Event selection

NPE18 triggered data was used from Run 12 $\sqrt{s_{NN}} = 193$ GeV U+U collisions, the database query was:

```
get_file_list.pl "grp(runnumber),sum(sanity),sum(events)"
-cond "production=P12id,trgsetupname=UU\_production\_2012,
filetype=daq\_reco\_MuDst,sanity=1,filename~st\_physics,tpx=1,emc=1,
storage!=hpss" -onefile -distinct -limit 0
```

The NPE18 trigger ID is 400203 for runs up to runno=13130033, 400213 in later runs. There are 8.77 M and 8.43 M events in these two triggers respectively. This corresponds to an integrated luminosity of 263.4 μb^{-1}.

The list of bad runs based on reference multiplicity that comes with Hiroshi's `RefMultCorr` class was used[1] [3]. These runs are the followings:

13117026	13117027	13117028	13117029	13117030	13117031	13117032
13117033	13117034	13117035	13117036	13118009	13118034	13118035
13119016	13119017	13129047	13129048	13132047		

Distributions of numbers of NPE18-triggered events compared to MB and ratios are shown in Fig. 1 by run number.

1.2 Reconstruction-level cuts

Reconstruction was done using an adopted version of the `StL0UpsilonMaker` class, with the SL12d libaries. See Sec. A.1 for details.

During the reconstruction, certain preselection conditions are applied, which are intended to keep most of the candidates but reduce the output size. The outline of the reconstruction is as follows:

- In the BEMC, look for energetic (DSMADC$\geq$18) tower that could have fired the trigger ("seed").
- Find good reconstructed tracks with p_T>0.2 GeV/c and $-2 < n\sigma_e < 3$. The following quality cuts are applied: $nHitsFit > 20$, $nHitsFit/nHitsPoss > 52$; $0 < trackflag < 1000$, $trackflag \neq 701$, 801 or 901; $0 < dE/dx < 6$ keV.

[1] Although the needed text files are there, Run12 U+U is not enabled within the class by default. It has to be added by hand

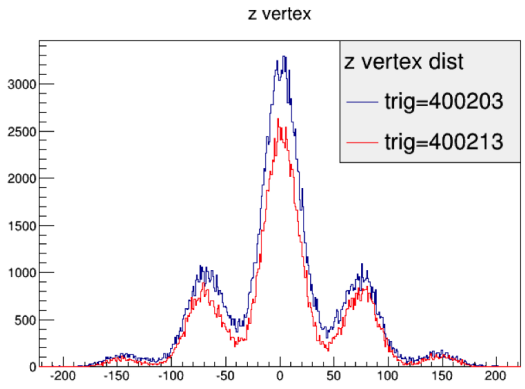

Figure 2: Z vertex distributions for the NPE18 trigger ID's 400203 and 400213.

- Clusterize energy around the seed by finding the two most energetic towers within the neigbouring 8 towers ($E_{clus} = E_{tower} + E_{tower2} + E_{tower3}$). The triggered candidate is required to have $p > 1$ GeV/c and $E_{clus}/p < 3$ c.
- Find a pair electron candidate cluster from the same vertex with a similar method (but allow any p and $E_{\rm clus}/p$.)
- Calculate the invariant mass M from the momentum, and keep candidates with $5 < M_{ee} < 20$ GeV/c^2 in order to reduce the size of the stored data sample

After all these selections, 401556 candidates remain.

1.3 Analysis cuts

The analysis was done using `StUpsilonAnalizer`, detailed in A.2. The following cuts were used on the ntuple level:

- **No Z vertex cut** was applied. Distributions for the NPE18 triggered data are shown in Fig. 2. A usual |zvertex|<50 cm would decrease statistics by 46%, which cannot be afforded by the low Υ production rate.
- Centrality determination was based on RefMultCorr [3]. The class was used as an afterburner to correct multiplicity. An overall RefMultCorr>47 cut was applied, corresponding to 0–60% centrality. The 0–10%, 10–30% and the 30–60% centrality bins correspond to RefMultCorr>465, 465≥RefMultCorr>230 and 230≥RefMultCorr>47, respectively. The actual values for $N_{\rm part}$ and $N_{\rm coll}$ are from Ref. [5].
- Rapidity of the Υ candidate is $|y| < 1$.
- Matching of $R < 0.04$ is required for both candidates in the BSMD
- Both electron candidate tracks are required to fulfil $-1.2 < n\sigma_{\rm e} < 3$.
- E/p ratios $0.75 < E_{\rm clus}/p < 1.4$ for both clusters
- Compactness $E_{\rm tower}/E_{\rm clus} > 0.7$ for triggered, and $E_{\rm tower}/E_{\rm clus} > 0.5$ for paired cluster.
- A global $p_{\rm T} < 10$ GeV cut is applied. Since we have virtually no Υs above the limit, this has ≈100% efficiency for signal, but still has background rejection power.
- An elecron pair opening angle cut $\cos(\vartheta)$>0 was investigated, but it was found to provide marginal benefits only and therefore was not utilized in the analysis.

The effects of these cuts are discussed in details in Sec. 3.

2 Peak extraction

The invariant mass spectrum was reconstructed for e^+e^-, e^+e^+ and e^-e^- pairs. Like-sign combinatorial background was determined as $N^{++} + N^{--}$.

2.1 Fitting

A simultaneous fit using the `RooFit` package [6] was used, similarly to the $\sqrt{s}$=500 GeV p+p analysis [2] was used in the following manner. The combinatorial background contribution was earlier found to be well described by a double exponential. In the peak region there is also a significant contribution of correlated background from Drell-Yan and open $b\bar{b}$ processes. Three Crystal-ball templates were used for the $\Upsilon(nS)$ peaks. Its parameters are obtained from embedded simulations. The Drell-Yan template is determined earlier from Pythia simulations to be well approximated by a $1/(1+m/m_0)^n$ shape [10]. The $b\bar{b}$ contribution were previously determined from Pythia to follow a $m^A/(1+m/B)^C$ model [11]. The likelihood on the fits of combinatorial background over like-sign points the full signal (combinatorial background + correlated background + three peaks) over unlike-sign points was maximized simultaneously. It is to be noted that the Drell-Yan and the $b\bar{b}$ shapes are very similar within the high-tower-triggered mass window. In order to increase the stability of the fit, only a single $1/(1+m/m_0)^n$ was considered in the final fit (ie. as if there was only Drell-Yan), thus reducing the number of parameters by 3. The absence of separate Drell-Yan and $b\bar{b}$ components was considered as systematics (see later).

Fig. 3 shows the fits for different centralities and p_{T}.

2.2 Bin counting

The Υ(1S+2S+3S) yield was determined by bin-counting within the range 8.8..11 GeV/c^2 and then subtracting the fitted background (combinatorial + correlated) contributions. The statistical error comes from *i)* the error on the background fit in the mass range, and *ii)* the pure statistical error ($\sqrt{N}$) over the peak count after background subtraction. These factors are square-summarized.

The Υ(1S) yield is determined with a similar method, within the range 8.8..9.8GeV/c^2 to minimize Υ(2S) contamination. There is no correction for the remainder Υ(2S) contamination since it is expected to be strongly suppressed. Instead, it is taken into account as a one-sided systematics (see Sec. 2.4.2).

Yields are listed in Tables 1, 2 and 3 for the Υ(1S+2S+3S), Υ(1S) and Υ(2S+3S) states together with the efficiency and uncertainties resulting from the fitting method.

2.3 Efficiency

With selecting the mass range 8..11 GeV/c^2, it could be avoided to pick up lot of fluctation from the Bremsstrahlung-range of the Crystal-ball shaped peaks. However, legitimate candidates are also lost. The mass-range cut efficiency is determined from embedding, by integrating the Crystal-ball shapes over the mass-range, normalized by the total integrals.

2.4 Systematics

2.4.1 Fitting systematics

The systematics of the peak extraction was extracted the following way.

- Move the lower edge of fit range from 6.6 to 8.0 GeV/c^2 in several steps
- Move the upper edge of fit range from 15.4..12.4 GeV/c^2 in several steps
- Move the peak position with 100 MeV (half the binwidth) up- and down
- Add an 50 MeV additional smearing to the peak (that is consistent with earlier p+p data with calibration issues and worse resolution)

[2] Note that the preliminary results [8] were obtained by first subtracting the combinatorial and then fitting the peak and correlated background together. The current method was chosen to be consistent with other analyses and to cancel corresponding systematics in R_{AA}. The background subtraction and the simultaneous fit methods yield consistent results [9].

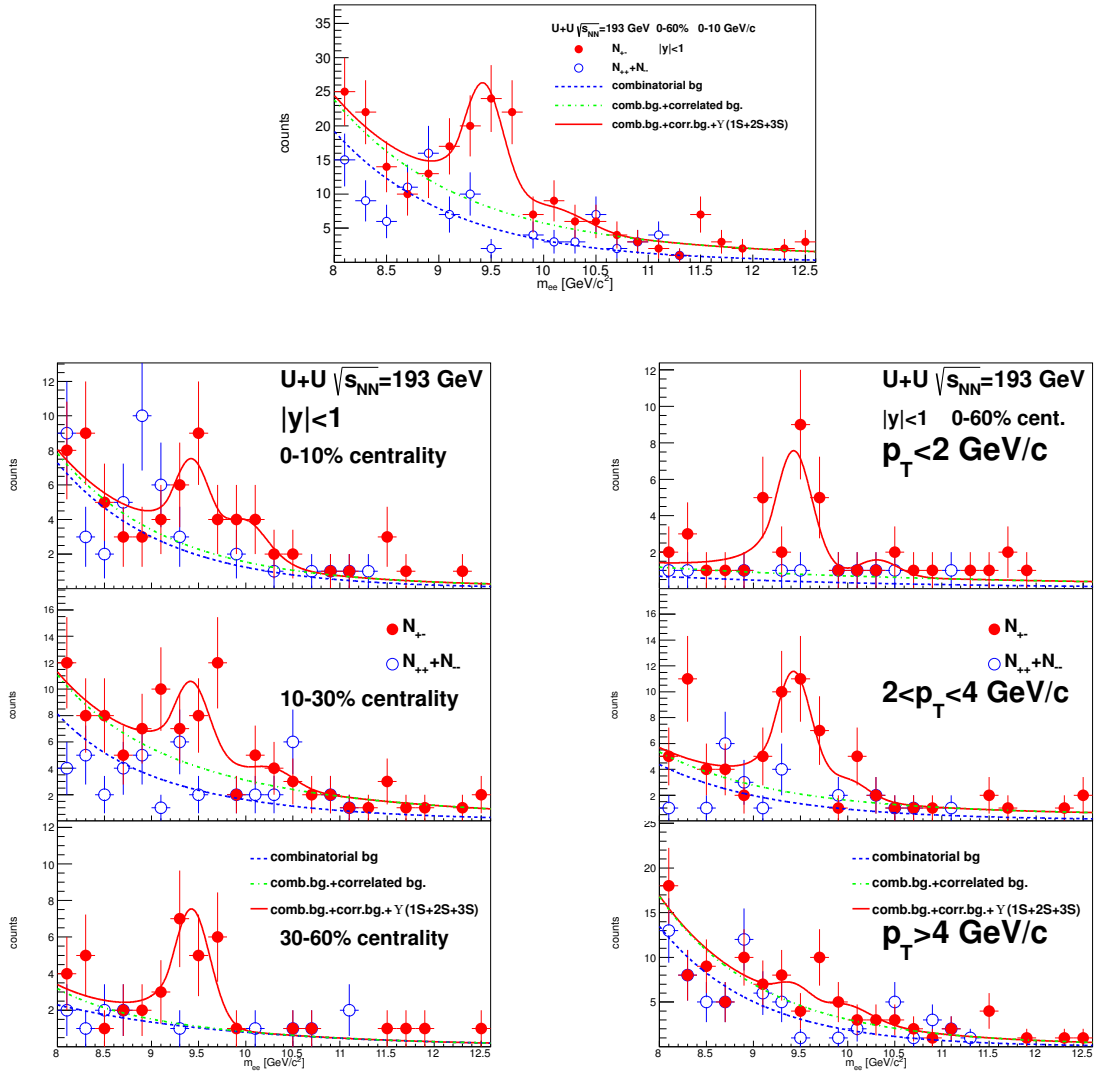

Figure 3: Invariant mass peak fits shown within the peak mass window. Top: All data in 0-60% centrality. Left column top to bottom: 0-10%, 10-30% and 30-60% centralities; Right column: $0< p_{\mathrm{T}} < 2$ GeV/c, $2< p_{\mathrm{T}} < 4$ GeV/c, $4< p_{\mathrm{T}} < 10$ GeV/c, respectively.

- Change CB composition method from $N^{++} + N^{--}$ to $2\sqrt{N^{++}N^{--}}$.
- Disable excited states $\Upsilon(2S)$ and $\Upsilon(3S)$
- Use $\bar{b}b$ shape instead of Drell-Yan shape for the correlated background
- Use $\bar{b}b$ shape added up to Drell-Yan shape with free normalization for the correlated background
- Use single exponential as combinatorial background instead of double exponential

These alterations are not independent at all: in fact they probe the stability of the same fit on the same dataset according to some aspects of the fitting algorithm. Therefore the errors are not summarized quadratically, but the maximum deviation is taken into account. In most bins, changing the fit range has the strongest effects. The peak position and resolution uncertainties, on the other hand, cause a large one-sided error in the case of separated Υ(1S) and Υ(2S+3S) states (since for instance a 50 MeV/c^2 uncertainty in the peak position is equivalent with moving the peak separation cut up and down with the same amount).

2.4.2 Υ(1S) peak excited state contamination

The Υ(1S) peak extraction efficiency is done similarly as above. It is likely that excited states 2S and 3S are strongly suppressed, as in Au+Au. However, these can yield some contamination, which is at maximum if the p+p 1S/2S, 1S/3S ratios are retained. This was calculated by integrating the 2S Crystal-Ball shape from embedding, normalized to 1S with the p+p 1S/2S ratio.

range (1S+2S+3S)	mass cut eff.	bin counts	stat. err.	bg.fit err.	syst. min	syst. max	comb. bg. fit	corr. bg. fit
0–60%	0.88	63.8	±8.5	±14.2	59.1	68.4	45.3	29.3
0–10%	0.89	20.3	±4.8	±7.1	17.3	20.7	17.3	3.5
10–30%	0.89	26.1	±5.4	±10.8	23.3	28.5	21.4	17.3
30–60%	0.87	17.9	±4.5	±5.4	13.2	21.7	9.8	0.7
p_T<2	0.88	23.9	±5.2	±8.5	20.1	24.7	3.8	4.2
2<p_T<4	0.88	29.4	±7.3	±10.4	25.0	31.7	12.2	7.8
4<p_T	0.90	15.6	±4.4	±11.7	13.0	16.5	27.5	14.3

Table 1: Υ(1S+2S+3S) results of peak fits. Mass cut efficiency, mass cut corrected peak counts ($\epsilon_{mass}N$), statistical error on counts ($\sqrt{N}$), errors from background fitting, peak extractions systematics lower and upper bounds, fitted counts of combinatorial and correlated backgrounds are listed respectively.

range (1S)	mass cut eff.	bin counts	stat. err.	bg.fit err.	syst. min	syst. max
0–60%		58.5	± 8.3	±15.0	55.3	65.8
0–10%		14.6	±4.2	±7.6	12.5	14.6
10–30%		24.5	±5.4	±11.4	22.9	25.6
30–60%	0.84	19.8	±4.8	±5.6	16.7	22.7
p_T<2		21.2	±5.0	±8.9	19.3	21.4
2<p_T<4		27.5	±5.7	±10.9	25.8	29.2
4<p_T		13.1	±3.9	±12.7	11.7	13.8

Table 2: Υ(1S) results of peak fits. Mass cut efficiency, mass cut corrected peak counts ($\epsilon_{mass}N$), statistical error on counts ($\sqrt{N}$), errors from background fitting, peak extractions systematics lower and upper bounds, fitted counts are listed respectively. (Uncertainties do not include excited state contamination.)

range (2S+3S)	mass cut eff.	bin counts	stat. err.	bg.fit err.	syst. min	syst. max
0–60%	0.54	11.5	± 4.6	± 2.58	8.44	20.9
0–10%	0.44	8.20	± 4.34	± 2.88	6.41	9.79
10–30%	0.64	6.02	± 3.05	± 0.91	4.93	10.31
30–60%	0.39	-2.97	± 2.75	± 1.39	-4.65	-0.49
p_{T}<2	0.75	3.90	± 2.28	± 3.00	1.99	6.92
2<p_{T}<4	0.42	8.50	± 4.52	± 2.22	5.70	9.89
4<p_{T}	0.46	2.95	± 2.52	± 8.55	-0.85	5.44

Table 3: Υ(2S+3S) results of peak fits. Mass cut efficiency, mass cut corrected peak counts ($\epsilon_{mass}N$), statistical error on counts ($\sqrt{N}$), errors from background fitting, peak extractions systematics lower and upper bounds, fitted counts are listed respectively. (Uncertainties do not include 1S state contamination.)

2.4.3 Impact of Υ(1S+2S+3S) peak composition on efficiency

The reconstruction efficiencies slightly differ for the states Υ(1S), Υ(2S), Υ(3S), with the excited state efficiencies being generally $\approx$ 10% greater than the ground state. The efficiencies for each state are discussed in Sec. 3 and the results are listed in Tables 11, 12 and 13. The Υ(1S+2S+3S) peak is a compound of these three states. Therefore the contribution of individual states has to be separated. The fit results from the Υ(1S), Υ(2S), Υ(3S) templates are listed in Table 4. It is to be noted that the Υ(3S) state never even has 1-σ significance, and it is very much anticorrelated with Υ(2S), and the Υ(1S) and Υ(3S) states do not really interfere. Moreover, the efficiency of the two excited states are close to each other. Therefore these two excited states were handled together. Estimating systematics (also in Table 4) was done by repeating the calculations by changing the excited state fraction so, that the Υ(2S) contribution is *i)* 1-σ higher for the upper limit, or *ii)* 1-σ lower but not below zero, for the lower limit.

range	Υ(1S)		Υ(2S)		Υ(3S)		syst−	syst+
0–60%	52.0	±10.5	6.61	±7.15	4.80	±6.18	1.1	1.5
0–10%	14.1	±5.57	7.48	±4.52	1.00	±3.34	2.4	3.9
10–30%	18.5	±6.98	1.65	±5.16	4.05	±4.67	2.8	4.7
30–60%	19.0	±5.34	0	±1.48	0	±1.67	0.3	0
p_{T}<2	19.9	±5.27	0	±5.63	3.17	±2.89	3.4	2.9
2<p_{T}<4	27.2	±6.73	5.03	±4.20	0.34	±8.37	0.2	0.3
4<p_{T}	5.88	±6.07	4.92	±5.20	1.20	±4.18	0.2	0.1

Table 4: Υ(1S), Υ(2S) and Υ(3S) peak range integrals and their errors from the simultaneous fit. The corresponding systematics lower and upper bounds are also listed (%).

3 Corrections and systematics

3.1 Trigger and vertex finding

No coincidence of the L0 trigger with the ZDC trigger was required. No L2 trigger was applied. In the 2010 Au+Au analysis, the MINUIT algorithm ensured that 99.93% of triggered events had a valid vertex [2]. The Υ candidates, with at least two energetic hits in the BEMC required, and with typically higher multiplicity, are expected to correspond to an even higher vertex finding efficiency. The 2012 U+U used largely the same reconstruction, therefore the vertex finding efficiency loss is expected to be way below 1% so it was neglected.

3.2 Geometrical acceptance

The geometrical acceptance is determined as part of the efficiency corrections via embedding, described in Sec. B.1. Its uncertainty comes from two sources: *i*) the fluctuating number of bad/excluded hot towers

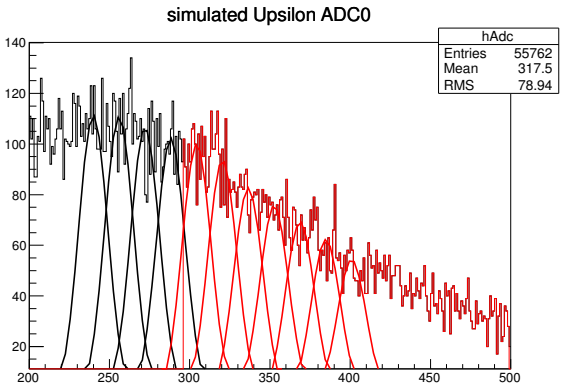

Figure 4: The adc0 distribution from J/ψ electron data, compared to Gaussian fits to the individual adc0|DSMadc=const distributions. The Gaussians are normalized in a 20 adc0 counts wide window each. The red Gaussians represent hits that would fire the trigger, while the black Gaussians would not. The red part of the histogram with an equivalent area to the red Gaussians begins at adc0=297.

in the given run, and *ii*) the uncertainity from the unknown polarization of the Υs. It was estimated in the analysis of Ref. [2] that the latter is the dominating effect. Since the same extrema apply to U+U as to Au+Au (or p+p), the same uncertainty of $(+1.7/-3.0)\%$ is assigned to acceptance determination in this analysis. The acceptance error is considered fully correlated between species.

3.3 Trigger turn-on systematics

The trigger cutoff is at DSMadc=18. However, the simulation applies cuts in ACD (adc0). The ADC-to-energy conversion may also differ in data and simulations. These two effects were estimated.

3.3.1 DSMadc vs adc0

The DSMadc>18 cutoff is usually associated with an adc0>303 value. However, adc0|DSMadc=const distributions are Gaussians with a final width $\sigma = 9$ as determined in Sec. D.4. Fig. 4 illustrates how the adc0 distribution is built up from single adc0|DSMadc=const distributions. Calculating the integrals of adc0|DSMadc=const distributions for each DSMadc>18 value reveals that the trigger treshold actually corresponds to adc0>297. Therefore this value was used in the embedding for efficiency determination. In the simulation verification of Sec. D.2, where the adc0=303 cutoff was used, this may cause a 1.5% relative difference on efficiency, translating into a 0.2% absolute difference, which is far within systematics and thus neglected.

It is found that the change in parameters within their errors (see Sec. D.4) cause a change which is smaller than an adc0 count in any case, so the systematics on adc0↔DSMadc conversion was considered as 1 adc0 count.

3.3.2 adc0 vs. $E_{\rm tower}$

The data and embedding mean and RMS of the adc0($E_{\rm tower}$) are determined from distributions listed in Sec. D.4 for regions below and above the trigger-turn-on energy regime. The means and RMSes are then interpolated with several functions for both data and embedding. The interpolations are shown on Figs. 5, 6. The difference in adc0 values of the embedding and data is taken at the average turn-on energy location $E_{\rm tower} = 4.6GeV$. See Tab. 5. The most difference in the case of means when interpolated with a 2nd order polynomial is a shift of 4 in adc0 counts in data trigger turn-on compared to embedding. The impact of rms distributions on the adc0 counts is negligible.

The possible adc shifts are added up linearly since they are not necessarily independent. The effect on a possible shift in adc0 value is then translated to changes in efficiency by running the embedding with different cutoffs. The systematic uncertainty on the Υ yields is listed in Table. 6.

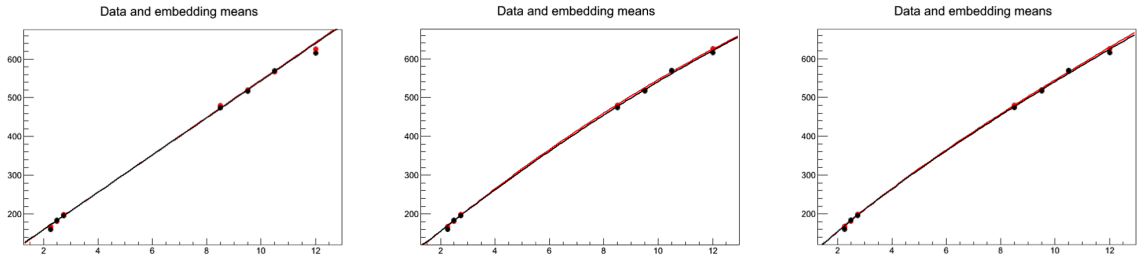

Figure 5: adc0(E_{tower}) distribution mean values for data (black) and simulation (red) points interpolated with linear (left), 2nd order polinomial (mid) and x^{α} (right) functions into the trigger turn-on range.

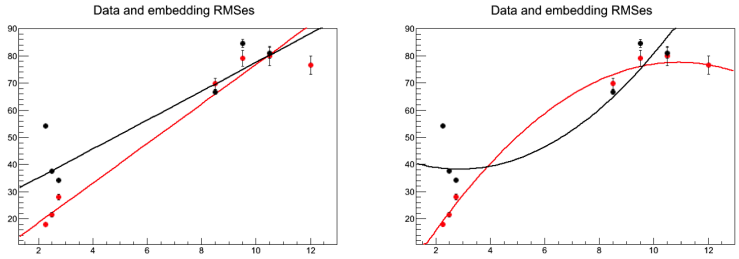

Figure 6: adc0(E_{tower}) distribution RMS values for data (black) and simulation (red) points interpolated with linear (left), and 2nd order polinomial (right) into the trigger turn-on range.

3.4 Tracking efficiency

Tracking efficiency error is taken from the analysis of Ref. [2]. The value $2 \times 5.88\%$ was used, considered to be totally correlated for the two tracks. As a conservative choice, it is not considered correlated between species since running conditions of the TPC could change. The efficiencies for a single electron are listed in Table 11.

3.5 TPC electron identification

The TPC electron ID cut of $-1.2 < n\sigma_{\text{e}} < +3$ was used in the analysis. The variable $n\sigma_{\text{e}}$ is constructed so that the electrons' distribution in it should follow a normal distribution (Gaussian, $\sigma = 1$, $mean = 0$) at any given momentum. However, it is not completely true – many analyses in U+U found that the actual $n\sigma_{\text{e}}$ distributions of electrons may slightly be narrower, and are centered at -0.5. Therefore the efficiency has to be estimated by isolating the electron contribution and comparing its integral within the cuts to the total integral. The efficiency was estimated the following ways:

1. Identified electron samples from NPE18 data using a single track reconstruction maker, described in Sec. C.4. The resulting $\epsilon(p)$ values were fitted with a line to interpolate smoothly.

2. Identified electron samples prepared for the MinBias J/ψ in U+U analysis [16]. The $\epsilon(p)$ values were given in variable binwidths. After unification into the wider, 1 GeV p bins the points were fitted with a line to extrapolate/interpolate smoothly.

3. A photonic electron analysis prepared for the NPE18 triggered J/ψ in U+U analysis, as described in Sec. C.5. The resulting values, in p_{T} bins, were used directly after p_{T}-weighting.

These methods yield a consistent result. The cleanest samples, with the smallest systematics achievable, are that of method no. 3, hence values from the latter were used. The M<150 MeV selection was used in error estimation since the statistical errors are smaller. Means, sigmas of the fit and efficiencies by p_{T}-bin are shown on Fig. 7. The single identified efficiencies from NPE and MB data are shown in addition in Fig. 8 The efficiencies are calculated in each centrality and p_{T}-range by properly p_{T}-weighting the single electron selection efficiencies (see Sec. B.5). The systematics were estimated by varying pushing means

ADC(E=4.6 GeV)	data	embedding	equivalent ADC shift
mean, linear fit	283.5	283.5	<1
mean, 2nd order poly fit	291.5	294.6	4
mean, x^α fit	293.3	295.0	2
RMS, linear fit	48.8	37.4	<1
RMS, 2nd order poly fit	40.7	46.7	<1

Table 5: Fit values evaluated at E=4.6 GeV and equivalent ADC shift

range	adc0 shift from DSMadc↔adc0	adc0 shift from adc0 ↔ $E_{\rm tower}$	adc0 shift linear sum	syst+ % (rel.)	syst− % (rel.)
0–60%				+1.1	−3.6
0–10%				+2.0	−3.4
10–30%				+0.8	−4.2
30–60%	±1	+4 / −1	+5 / −2	+0.9	−2.6
$p_{\rm T}$<2				+2.3	−2.7
2<$p_{\rm T}$<4				+0.7	−1.6
4<$p_{\rm T}$				+1.0	−1.6

Table 6: Systematics corresponding to possible adc0 shifts from understanding DSMadc↔adc0 and adc0↔ $E_{\rm tower}$ conversions.

and sigmas in each $p_{\rm T}$-bin to their maxima or minima within the region allowed for the errors, doing the $p_{\rm T}$-weighting and selecting the minimal and maximal values for the recalculated efficiencies. The M<50 results are consistent far within the limits of systematic variations, and differences using this selection is not added up to the systematics. Values computed for different centrality and $p_{\rm T}$ ranges are summarized in Table 7. The efficiencies for each state are listed in Tables 11, 12 and 13.

3.6 TPC-BEMC matching

.

The matching efficiencies were established from embedding. The efficiencies for each state are listed in Tables 11, 12 and 13. In order to estimate systematics, the embedding was compared to photonic electron enhanced real data, as detailed in Sec. D.1. The ratio of the two is close to unity and the contamination in the data sample is unknown, therefore no further correction was applied. Instead, $|1-\epsilon_R^{data}/\epsilon_R^{embedding}|$ was treated as systematics in each p-bin. Along with $R<0.04$, $R<0.035$ and $R<0.045$ was investigated to test the stability of efficiencies, and essentially no difference was found. Cut efficiency comparison of simulation and data is shown in Fig. 9 The resulting systematics are shown p-weighted in Table 8.

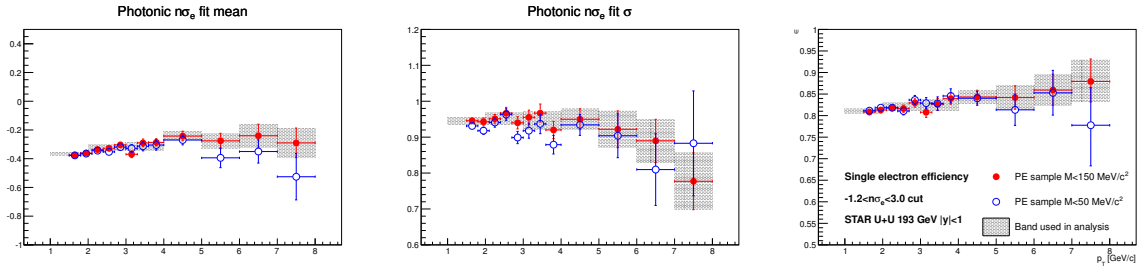

Figure 7: The mean (*left*) and the width (*center*) of the photonic electron $n\sigma_{\rm e}$ fits in p-bins, as well as the computed corresponding efficiency of the $-1.2<n\sigma_{\rm e}<+3$ cut (*right*). Red points correspond to PE selection with M<150 MeV, blue points to M<50 MeV. The shaded bands represent systematics. Its center value was used in the analysis in each $p_{\rm T}$ bin.

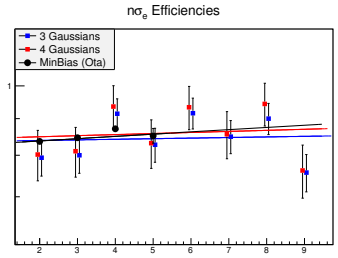

Figure 8: Fitted efficiencies from single identified NPE18 (3 and 4-Gaussian, red and blue respectively) and photonic Minimum Bias electrons (black) bin-by-bin. A linear fit is laid over the points. (A vertical tick is 10%.)

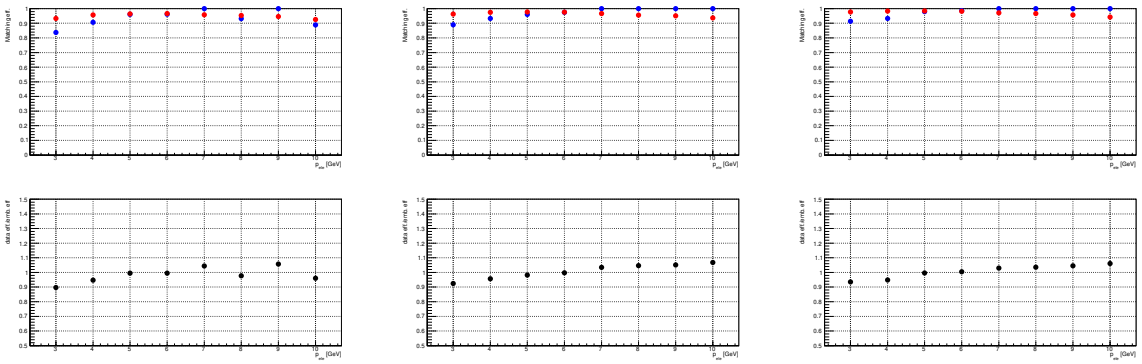

Figure 9: Efficiencies from embedding (red) and photonic-enhanced electron sample (blue), and efficiency ratios $\epsilon_R^{data}/\epsilon_R^{embedding}$ (black), for $R < 0.035$, $R < 0.040$ and $R < 0.045$ (left to right) for electrons in 1 GeV/c wide momentum bins.

range	M<150	stat.max.	stat.min.	M<50	3-gaus	4-gaus	MinBias	syst+	syst−
0–60%	84.2	82.5	86.9	83.8	84.5	86.0	86.2	+2.0	−3.3
0–10%	84.2	82.5	86.9	83.8	84.5	86.0	86.2	+2.0	−3.3
10–30%	84.2	82.5	86.9	83.8	84.5	86.0	86.2	+2.0	−3.3
30–60%	84.2	82.5	86.9	83.8	84.5	86.0	86.2	+2.0	−3.2
p_{T}<2	84.2	82.5	86.5	84.2	84.5	86.0	86.1	+1.9	−2.8
2<p_{T}<4	84.0	82.5	86.9	83.6	84.5	86.0	86.2	+1.9	−3.8
4<p_{T}	84.6	82.6	88.2	83.0	84.6	86.2	86.6	+2.4	−4.2

Table 7: The p_{T}-weighted single-electron $n\sigma_{\mathrm{e}}$ efficiencies (%) by centrality and p_{T}-range, extracted from photonic electrons with M<150 MeV. Maxima and minima for systematic variations within statistical errors are listed, as well as cross-checks with photonic selection criterion M<50 MeV, cross-checks with NPE-triggered TPC-identified electrons fitted with 3 and 4 Gaussians, and cross-checks with photonic electrons from the Minimum Bias data J/ψ analysis [16]. The last two columns show the systematic error percentages (%) that envelope all the above variations.

range	syst
0–60%	2.7
0–10%	2.8
10–30%	2.6
30–60%	2.7
p_{T}<2	2.6
2<p_{T}<4	2.4
4<p_{T}	2.4

Table 8: Matching systematics

3.7 Electronness cut E_{clus}/p

While most of high-p_{T} hadrons are MIPs, electrons are expected to deposit all or most of their energy in the calorimeter and therefore have $E_{\mathrm{clus}} \approx p$.

3.7.1 Cut position

The efficiency versus different cut positions with a cut window width of 0.65 is shown in Fig. 10. The final $0.75 < E_{\mathrm{clus}}/p < 0.40$ cut was selected because it falls close to the top of the curve, but a little left from it where there is no suddenly changing behavior in the data, or in the embedding at any centrality.

The cut on the corrected E_{clus}/p is shown on Fig. 11 versus event multiplicity.

3.7.2 Parametrization of momentum dependence

The efficiency is generally estimated using simulated Υ decays embedded into real U+U data. It was found that embedding does not reproduce E_{clus}/p properly [7]. This is less of a problem in the case of precedent analyses where a not too tight cut is applied on the triggered electron candidate only. In the analysis, however, a relatively tight cut had to be applied in order to suppress background from hadrons.

Well identified TPC-electron samples as well as photonic electron enhanced samples were used to parametrize the dependence of the E_{clus}/p distribution dependence in 1 GeV/c momentum bins. See the individual distributions in Figs of Sec. D.2.

The Gaussian fit peak and width parameters are shown on Fig. 12.

In the case of means, the momentum dependence of embedding was parametrized using a power law function $a + b/x^c$ ($a = 0.985658, b = 1.28574, c = 1.5326$ with Minuit) [3] . The sigmas were parametrized by a second order polynomial ($a = 0.284058, b = -0.0332729, c = 0.00145409$ from Minuit).

The data was parametrized with a power-law including an additional exponentional cutoff to describe the low-p behaviour seen in the photonic data: $a+be^{-dx}/x^c$. An upper and lower limit of the parameters

[3] It is important to note, that decay electrons from the Υ are distributed mostly in the middle bins: over 90% is in four bins from 3.5–7.5 GeV/c (see Sec. B.5).

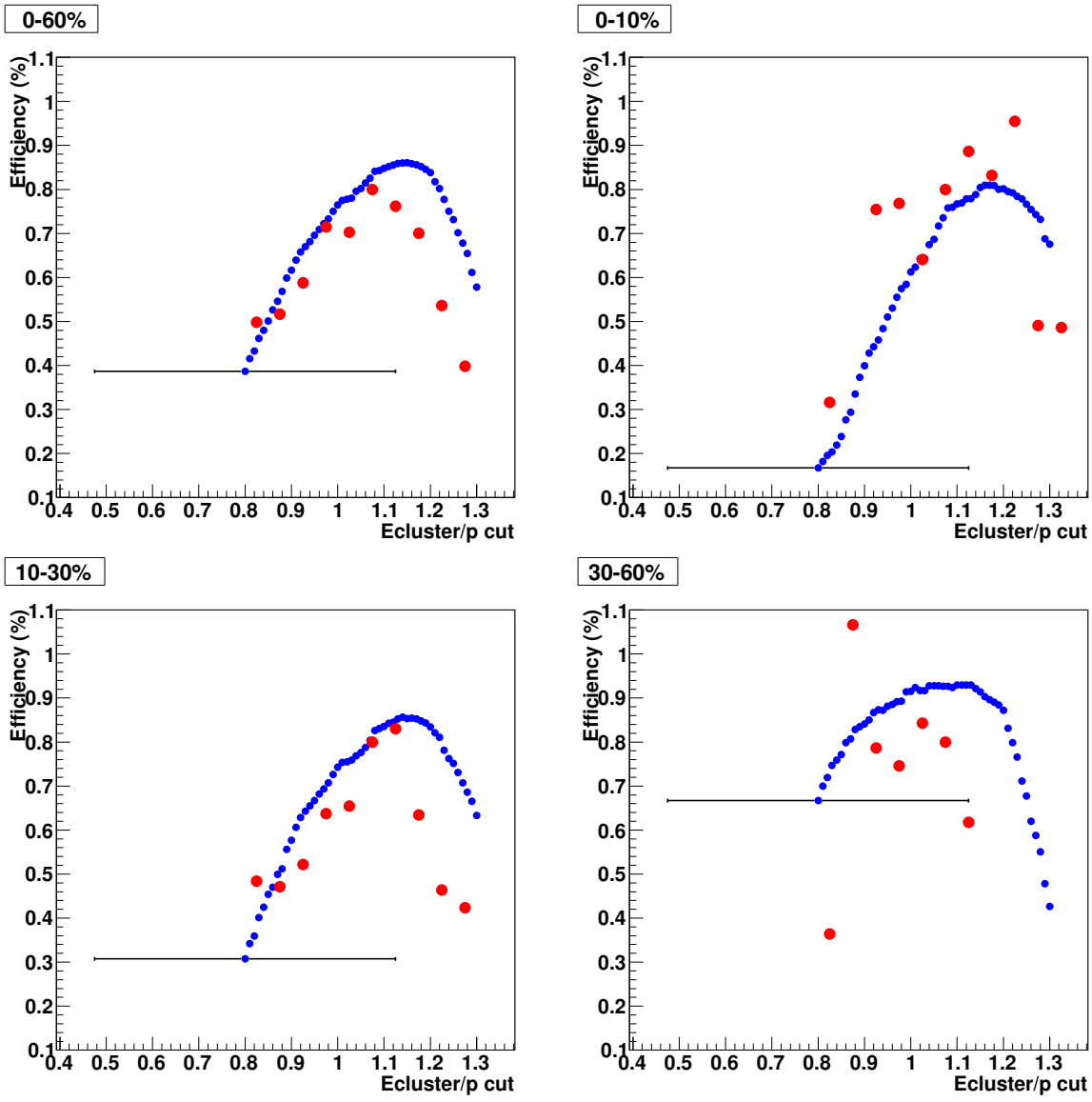

Figure 10: Blue points: Uncorrected embedding efficiency of an $(x - 0.325) < E_{\rm clus}/p < (x + 0.325)$ cut w.r.t. cut position x for 0-60%, 0-10%, 10-30%, 30-60% centrality bins. (Note that the efficiency does not depend strongly on $p_{\rm T}$.) Red points: Υ peak counts arbitrarily normalized, from real data, after the cut applied. The horizontal error bar represents the width of the cut window.

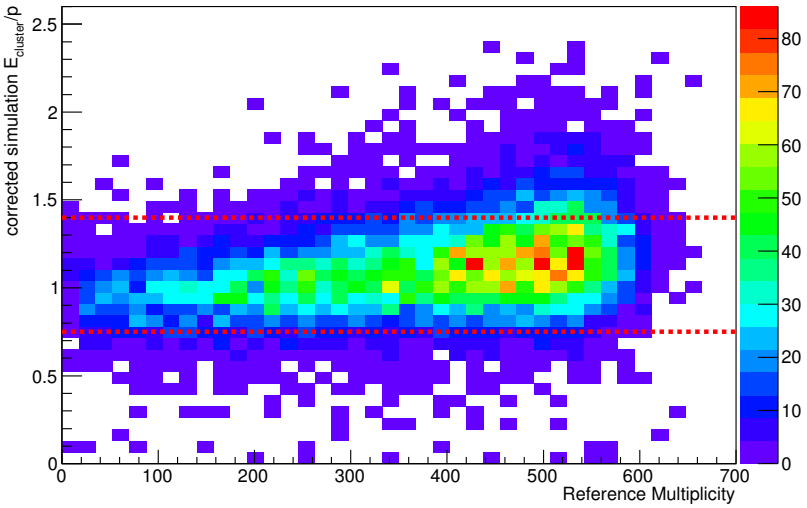

Figure 11: The $E_{\rm clus}/p$ distribution versus reference multiplicity, determined using corrected simulation. The two horizontal dashed lines represent the cut.

was determined the following way:

- A summed-up sample was produced from the TPC and photonic-enhanced identified samples. In bins where both samples are present, an arithmetic weighted average was produced with $w_i = 1/\delta_i^2$) weights. This was to account for behavior in the low momentum range where only photonic sample is present. Since the gaussian parameters of photonic fit are marginally consistent but overshoot the mean and sigma parameters with about 1-*sigma* of the TPC-identified sample, the goal was only consistency with the photonic points. Then the integral error over the central region 4-6 GeV was determined, and the function was scaled upwards with this value. The parameters are $a = 0.897421, b = 0.0603407, c = -4.4543, d = 1.1$.

- The lower limit was determined by first fitting the TPC-identified data points. Then the integral error over the central region 4-6 GeV was determined, and the function was pressed down with this value. Parameters are $a = 0.842708 b = 0.0540509 c = -3.87428 d = 0.9$. Note that parameter d was tuned by hand to achieve best containment of the lowest two points with high errors.

A very similar process was applied to data sigmas, with a simple second order polynomial parametrization, fit results being $a = 0.504926, b = -0.0932158, c = 0.00644878$ for thi upper, and $a = 0.389478, b = -0.0730774, c = 0.00512882$ for the lower limit. These parametrizations adequately contain and extrapolate tpc-identified points, and consistent with the trend marked by the photonic points.

3.7.3 Efficiency

Correction of the embedding was done with an afterburner (See Sec. B.1.1), feeding in the parametrized means and sigmas in. The average of the upper and lower systematic limit in case of real data were used as the „default“ value for the correction. The cluster energy was transformed on an entry-by-entry basis to reflect the new means and sigmas, by applying the following formula:

$$E_{\rm clus}^{corr} = E_{\rm clus}^{uncorr} + (\mu_{data} - \mu_{emb}) + (E_{\rm clus}^{uncorr} - \mu_{emb}) \times (\sigma_{data}/\sigma_{emb} - 1) \ .$$

The selection cuts were applied on the simulated data after applying the cuts for the L0 trigger, acceptance, track recognition, clustering and matching to obtain the efficiency.

The actual values of this correction for each state are listed in Tables 11, 12 and 13.

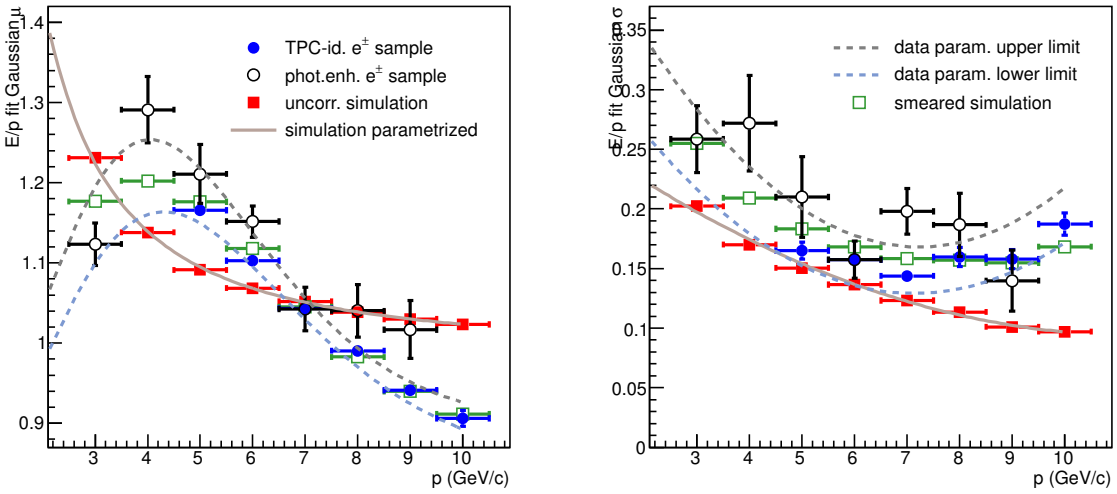

Figure 12: $E_{\rm clus}/p$ Gaussian peak parameters. Red points are uncorrected embedding. Blue points are TPC-identified data, black points are photonic-enhanced data. The continuous line is a parametrization of the momentum dependence of embedding, the dashed lines are a simple parametrization of the uncertainty band over data used for determining the correction. Green points are corrected embedding.

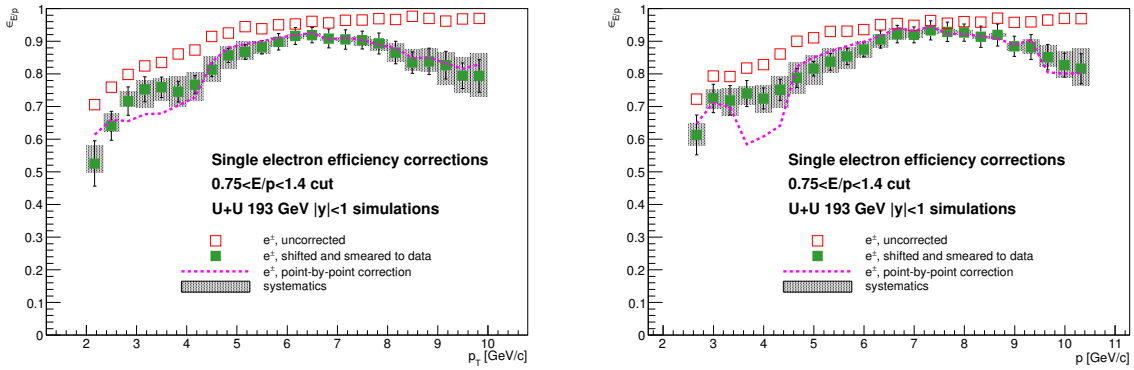

Figure 13: Single electron efficiency of the $0.75 < E_{\rm clus}/p < 1.4$ cut vs. $p_{\rm T}$ *(left)* and p *(right)*, as determined from uncorrected and corrected simulations. The statistical errors, shown on the corrected points, are similar on the uncorrected datasets. (This uncertainty does not directly enter the range-integrated Υ efficiency calculations.) The gray systematics band is from the uncertainty of the parametrization described in the text. The magenta line of point-by-point corrections is used as a cross-check in efficiency-determination.

3.7.4 Systematics

Systematics were obtained by comparing the corrections „default“ values of corrections with those using the upper or the lower limits[4]. As a cross-check, a discrete point-by-point corrections were also calculated: instead of the smooth curves, the arithmetic average of the data was compared to the embedding within each of the 1 GeV/c wide bins. The deviation of the efficiency obtained by this method and the smooth curve method is smaller than the systematics from the fit value bands. The only exception is the highest Upsilon p_{T}>4 GeV/c range.[5]. In this single range, the lower limit of the systematics was extended. However, it would be still inside a symmetrized systematics band.

The correction systematics are listed in Table 9.

range (p_{T} in GeV/c)	μ+ (%)	$\mu-$ (%)	σ+ (%)	$\sigma-$ (%)	pt-by-pt	syst+ (%)	syst− (%)
0–60%	5.4	2.7	3.7	3.5	3.6	6.6	4.4
0–10%	8.8	6.6	8.3	6.7	5.1	12.1	9.4
10–30%	6.5	2.5	3.7	3.5	3.3	7.5	4.4
30–60%	2.6	0.8	1.4	1.8	3.1	2.9	2.0
p_{T}<2	5.8	2.1	3.2	2.5	2.3	6.7	3.3
2<p_{T}<4	6.3	4.5	4.2	5.3	3.4	7.6	7.0
4<p_{T}	2.0	0.3	4.2	1.9	8.3	4.7	*3.7*

Table 9: Systematics on the E/p, from embedding E/p distribution mean and width correction uncertainties. The asymmetric errors from the two parameters are summed up quadratically, with the exception of the p_{T} >4 bin where the point-by-point deviations were taken.

3.8 Compactness cut $E_{\mathrm{tower}}/E_{\mathrm{clus}}$

Energy deposits even from a high energy electromagnetic particle are expected to be compact, with most of their energy in a single tower. Because of the low amount of data, cuts had to be tuned to have a high background rejection power and an acceptably high efficiency at the same time. It was found that a tuning with ≈90% to 95% efficiency is close to the optimum. Triggers select energetic towers and therefore candidates are biased towards even more compact clusters ($E_{\mathrm{tower}}/E_{\mathrm{clus}} \approx 1$) than those electrons that do not fire the trigger. Therefore a looser cut is needed then in the case of paired candidates to achieve the same efficiency.

3.8.1 Efficiency

The efficiency versus cut positions is shown in Fig. 14. The efficiencies for each state are listed in Tables 11, 12 and 13.

3.8.2 Systematics

The embedding was tested against the triggered candidate. The match is satisfactory. (Examples are shown in Sec. D.3.) Data and embedding efficiencies with the stricter cut at 0.7 were compared to TPC-identified, cluster-matched electrons ($n\sigma_{\mathrm{e}} < 3$, $n\sigma_{\pi} < 2$, $R_{SMD} < 0.04$), after p-weighting applied. The systematics is just calculated as the discrepancy between embedding and data. It is approximately 1% on one candidate. In the case the E_{clus}/p cut is also applied, similar but slightly higher values result. This increase is likely an effect of the E_{clus}/p issue of embedding, which is already accounted for in the systematics. Therefore the TPC-identified systematics were used. Both values are listed in Table 10. It is assumed that the uncertainty on the paired cluster is very similar since the efficiencies are set to be similar. It is also assumed to be completely correlated, therefore the systematics was multiplied by a factor of 2.

[4]Note that the upper limits on means and sigmas correspond to a smaller efficiency, or, stronger correction. On the other hand, „positive“ systematic error boundaries here mean a higher R_{AA}, that is, smaller corrections.

[5]Since the only point lying out of the the band is the p=3 GeV/c point, this is obvious, considered that high Upsilon p_{T} range is the only one where this bin has a remarkable weight, as seen on Fig. 23.

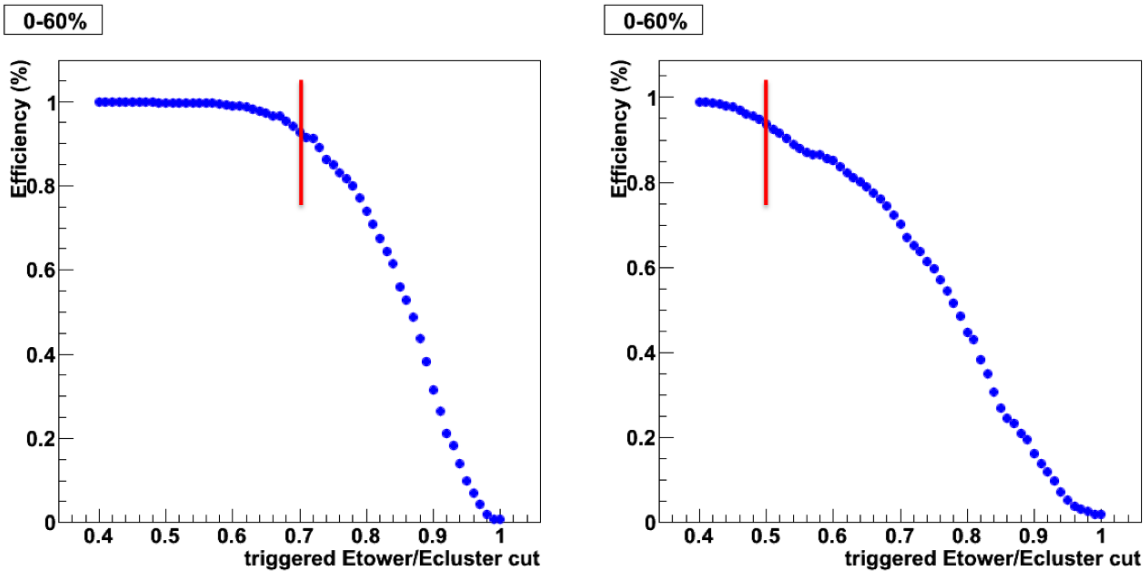

Figure 14: Blue points: Embedding efficiency of an $E_{\text{tower}}/E_{\text{clus}} > x$ cut w.r.t. cut position x for triggered (left) and paired (right) clusters. The cut position applied in the analysis is indicated by a red line.

range	TPC ID	TPC+EMC ID
0–60%	1.1	1.5
0–10%	1.0	1.5
10–30%	1.1	1.4
30–60%	1.1	1.5
p_{T}<2	1.1	1.7
2<p_{T}<4	1.1	1.4
4<p_{T}	0.6	0.8

Table 10: Compactness cut systematics (%) computed as $|embedding - data|/embedding$

3.9 Embedding weight systematics

The embedding p_{T} and y distributions were weighted according to Sec. B.3.

The slope parameter T of the p_{T} distribution was increased with $\Delta T = 0.021$ GeV, about the width σ of the measured slope, to reach the measured T.

The y width was changed from the fitted $\sigma = 1.15$ with 0.15 which covers the variations by fitting in range (see Sec. B.3), and also covers $\sigma = 1$, the value used by previous analyses [2].

The uncertainty on p_{T} weighting was added up quadratically to the uncertainty from decreasing or increasing the y width, depending on which one is larger for the given dataset. The values are listed in Table 14.

4 Analysis results

4.1 Production

4.1.1 Cross-section

After all the corrections, the Υ(1S+2S+3S), Υ(1S) and Υ(2S+3S) cross sections (times B.R.) in $\sqrt{s_{_{NN}}} = 193$ GeV U+U collisions at mid-rapidity are

$$B_{\text{ee}} \left.\frac{\mathrm{d}\sigma^{\Upsilon}_{AA}}{\mathrm{d}y}\right|_{|y|<1} = \left[4.02 \pm 1.05(stat)^{+0.83}_{-0.78}(syst)\right] \mu\text{b}$$

range	$\epsilon_{acc+trig+trk}$	ϵ_{match}	$\epsilon_{n\sigma_e}$	$\epsilon^{corr}_{E_{clus}/p}$	$\epsilon_{E_{tower}/E_{clus}}$	Total ϵ
0–60%	8.41	95.7	70.9	70.6	88.4	3.56
0–10%	6.2	93	70.8	54.8	81.3	1.82
10–30%	8.05	95.9	70.9	67.9	88.7	3.29
30–60%	13.4	97.9	70.9	87.3	91.7	7.41
p_T<2	7.66	96	70.8	68.7	89.4	3.2
2< p_T<4	8.93	95.5	70.6	73.2	88.2	3.89
4<p_T	10.2	95.3	71.6	70.3	85.3	4.18

Table 11: Υ(1S) reconstruction efficiencies excluding mass cut efficiency (%). Each value means cuts applied on both electron tracks/clusters.

range	$\epsilon_{acc+trig+trk}$	ϵ_{match}	$\epsilon_{n\sigma_e}$	$\epsilon^{corr}_{E_{clus}/p}$	$\epsilon_{E_{tower}/E_{clus}}$	Total ϵ
0–60%	9.33	93.9	70.9	72.8	89.6	4.05
0–10%	7.19	90.2	70.8	55.3	88.7	2.25
10–30%	8.99	95.7	70.9	73.8	89.8	4.04
30–60%	14.3	94.7	70.9	87.4	90	7.55
p_T<2	8.99	94.3	70.8	72.7	92.4	4.04
2< p_T<4	9.37	93.4	70.6	73.2	87.5	3.95
4<p_T	10.7	93.7	71.6	72.5	84.6	4.4

Table 12: Υ(2S) reconstruction efficiencies excluding mass cut efficiency (%). Each value means cuts applied on both electron tracks/clusters.

$$B_{ee}\left.\frac{d\sigma^{\Upsilon(1S)}_{AA}}{dy}\right|_{|y|<1} = \left[3.79 \pm 1.00(stat)^{+0.87}_{-0.91}(syst)\right]\ \mu b$$

and

$$B_{ee}\left.\frac{d\sigma^{\Upsilon(2S+3S)}_{AA}}{dy}\right|_{|y|<1} = \left[0.65 \pm 0.30(stat)^{+0.54}_{-0.21}(syst)\right]\ \mu b$$

respectively.

4.1.2 p_T-spectrum

Finite binwidth makes a rapidly falling spectrum appear flatter than it would be without any binning. In order to provide a p_T-spectrum, the effect of binning has to be reversed, a bin-shift correction has to be applied. Usually this is done with an iterative process, by

1. fitting the points with a properly selected curve $f(p_T)$.
2. calculating the bin corrections based on the integral of the function in a given bin and also globally, $c_i = \int_{x\in i} f(x)dx/f(\langle p_T\rangle)$, $c = \int_x f(x)dx/f(\langle p_T\rangle)$.
3. applying the correction bin-by bin, normalized with the global correction, to each bin content $N'_i = N_i(c/c_i)$, and also for their errors.
4. repeating from 1) until it converges. This is adequate in the case there are enough points with relatively small uncertainties.

In our case, however, an iterative process would be governed by the errors and thus would introduce a huge systematic factor on the fit. Instead, we used an a priori assumption of a Boltzmann-shape, $f(p_T) = \frac{p_T}{exp(p_T/T+1)}$ and then tested its consistency against our data. The $T = 1.16$ GeV was chosen based on a parametrized fit to experimental data on different c.m.s. energies, as described in [2] for the parametrization of embedding.

Fig. 15 shows the p_T-spectrum of Υ(1S+2S+3S) before and after the bin shift correction. The resulting fit for the spectrum after correction yields $T_{fit} = 1.36\pm0.23$, that is consistent to the assumption

range	$\epsilon_{acc+trig+trk}$	ϵ_{match}	$\epsilon_{n\sigma_e}$	$\epsilon^{corr}_{E_{clus}/p}$	$\epsilon_{E_{tower}/E_{clus}}$	Total ϵ
0–60%	9.31	94.5	70.9	75	87.4	4.08
0–10%	7.1	92.5	70.8	59.4	80.1	2.21
10–30%	9.2	93.8	70.9	75.7	88.8	4.11
30–60%	13.7	97.5	70.9	88.1	90.1	7.53
p_T<2	8.8	94.7	70.8	74.6	89.7	3.95
2< p_T<4	9.77	94.9	70.6	76.4	85.6	4.28
4<p_T	10.3	92.6	71.6	72.4	83.5	4.13

Table 13: Υ(3S) reconstruction efficiencies excluding mass cut efficiency (%). Each value means cuts applied on both electron tracks/clusters.

range	y-weighting syst	p_T-weighting syst−	p_T-weighting syst+	total weighting syst.
0–60%	0.7	2.0	2.0	2.1
0–10%	0.8	0.2	0.3	0.9
10–30%	0.8	3.0	3.7	3.8
30–60%	0.6	1.4	2.3	2.4
p_T<2	2.1	1.0	0.4	2.3
2<p_T<4	1.0	0.8	0.0	1.3
4<p_T	0.7	1.0	0.1	1.2

Table 14: Systematics on embedding distribution weighting. Either p_T-weighting syst− or syst+ is used, whichever is larger. The y-uncertainty is added up quadratically to it.

within uncertainties. Note that this error does not include systematics, which are partly correlated between different points.

Fig. 16 shows the p_T-spectrum of Υ(1S) before and after the bin shift correction. The resulting fit is the very similar $T_{fit} = 1.35 \pm 0.22$, suggesting that the production of different states is insensitive to the measurement's momentum selection.

4.2 Nuclear modification

4.2.1 The p+p reference

The same Run9 p+p reference is used as in the Au+Au analysis [2]. While the U+U collisions were taken at $\sqrt{s_{NN}} = 193$ GeV, the p+p reference is for $\sqrt{s_{NN}} = 200$ GeV. The two factors one has to take into account is the excitation function of the p+p total inelastic cross section, and of the Υ production cross section (both of which rise with energy). According to the calculations of Ref. [12], the difference of the of the inelastic cross sections at these two energies within the ALICE acceptance is in the order of 0.5-% ($\sigma^{inel}_{pp} \approx 42.5$ mb instead of $\sigma^{inel}_{pp} \approx 42.75$ mb). Another calculation [13] yields a similar value, 0.6% (difference between $\sigma^{inel}_{pp} \approx 40.46$ mb vs. 40.70 mb). The uncertainty on this number mostly comes from the extraction method (xyscan) and it is below 0.1% in absolute terms, therefore neglected, the correction value 0.5% was used.

There is a stronger dependence of the production cross section σ^{Υ} on the beam energy, shown in Fig. 9 of Ref. [14]. Besides this model, we used a purely data-driven method to control the uncertainties. The same measurements were fit with a linear function in the RHIC-LHC energy regime and found to yield a good description. Three different regimes were chosen (omitting points from both ends), and the results are found to be very similar. Fig. 17 shows the measurements, model and fits, table 15 lists the cross sections obtained from NLO CEM as well as the direct data fits.

The correction factor is determined as $cf = \frac{d\sigma^{\Upsilon}/dy|_{\sqrt{s}=200\text{ GeV}} - d\sigma^{\Upsilon}/dy|_{\sqrt{s}=193\text{ GeV}}}{d\sigma^{\Upsilon}/dy|_{\sqrt{s}=200\text{ GeV}}}$. There is no remarkable difference between the linear fits. The average correction factor from lines 1 and 2 of the table, $\overline{cf} = 0.0455$ was used in rescaling, multiplying the R_{AA} with $1/(1\text{-}\overline{cf})$. The error is taken as any $|cf - \overline{cf}| \approx 0.5\%$, which is neglected. The macro is described in Sec. A.5.

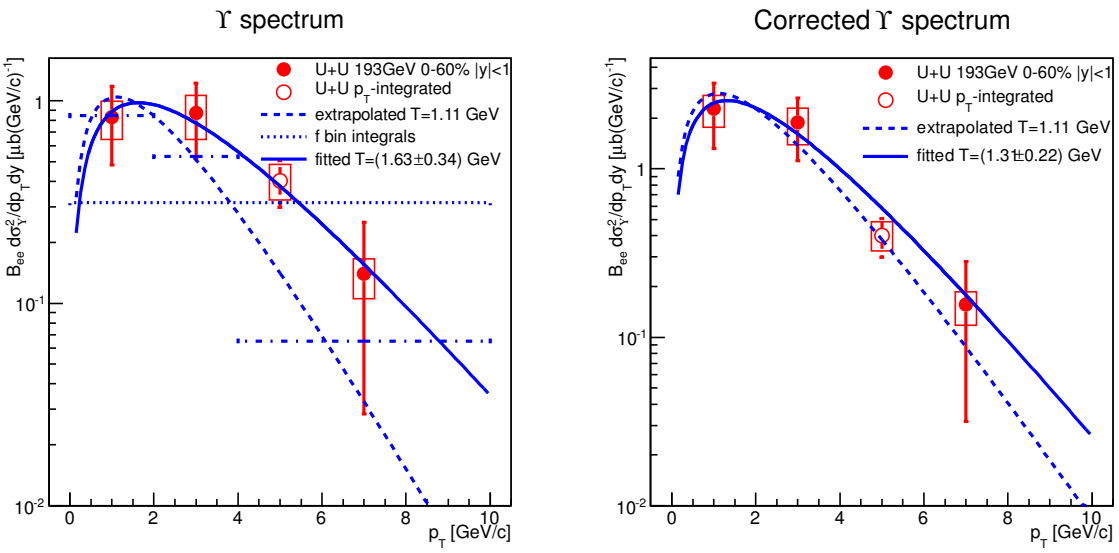

Figure 15: The Υ(1S+2S+3S) p_{T}-spectrum before (*left*) and after (*right*) bin shift correction.

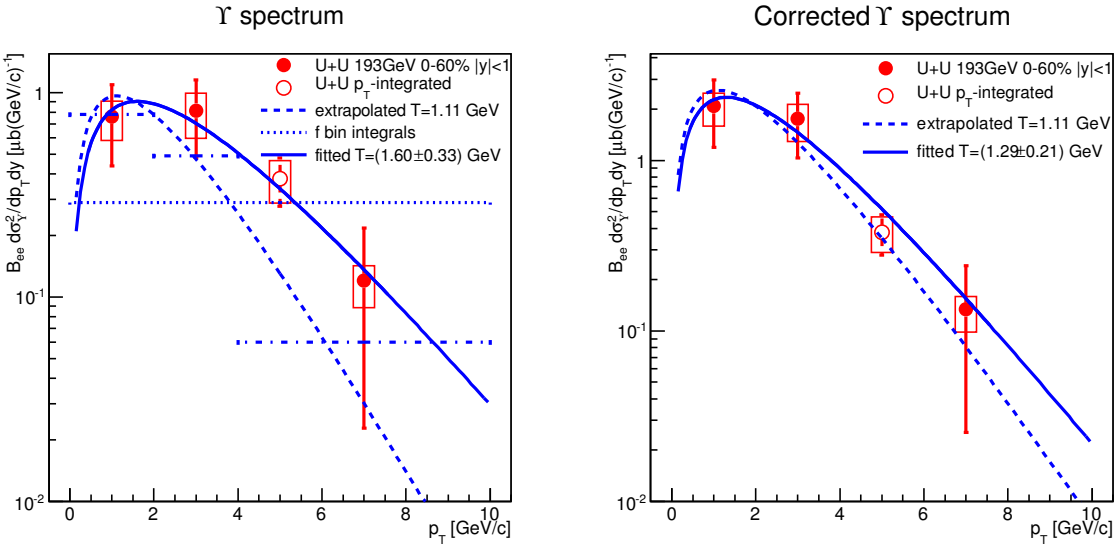

Figure 16: The Υ(1S) p_{T}-spectrum before (*left*) and after (*right*) bin shift correction.

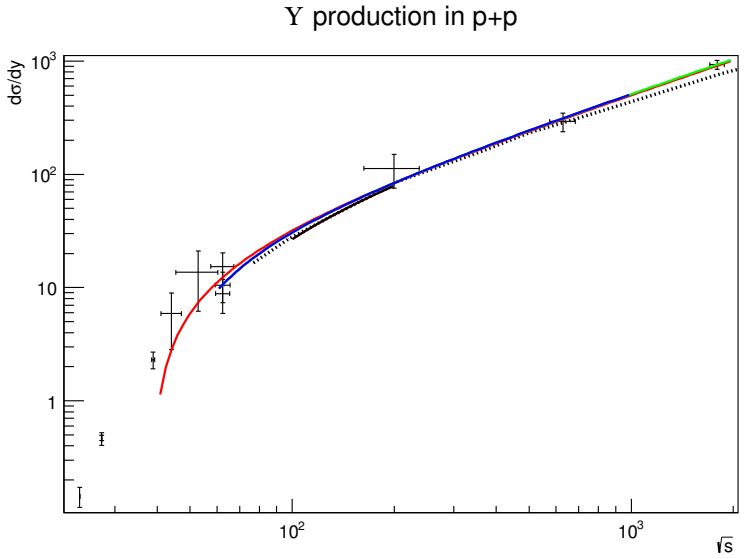

Figure 17: The measurements used in Fig. 9 of Ref. [14] compared to the NLO CEM model as well as to fits by linear function in the RHIC-LHC energy regime. The lines are explained in Table 15.

line on Fig. 17	color	$d\sigma^{\Upsilon}/dy\|_{\sqrt{s}=200\,\mathrm{GeV}}$	$d\sigma^{\Upsilon}/dy\|_{\sqrt{s}=193\,\mathrm{GeV}}$	cf
NLO CEM	black	79.2244	75.5423	0.0464763
linear fit 60 GeV – 2 TeV	green	83.7693	80.0468	0.0444384
linear fit 40 GeV – 2 TeV	red	83.6439	80.0162	0.0433707
linear fit 60 GeV – 1 TeV	blue	83.8257	80.1003	0.0444420

Table 15: Evaluated fit results on the $d\sigma^{\Upsilon}/dy$ denpendence on $\sqrt{s}$, and the correction factor for the reference.

4.2.2 Number of collisions

The N_{coll} values used for R_{AA} calculation are listed in Table 16. The values are computed from [4]. The relative errors on N_{coll} in each centrality bin were determined in the following manner: an estimate on different binning is specified in Ref. [18]. The main source of systematics is the p+p cross-section. The Phobos Glauber Monte Carlo v1.1 [19] was tuned by changing the cross-section to approximately reproduce the above errors, and then the errors for the wider bin were computed with the same code.

range	N_{coll}	error	relative error (%)
0–60%	459	10	2.2
0–10%	1146	49	4.3
10–30%	574	41	7.5
30–60%	154	37	2.4

Table 16: List of N_{coll} values and uncertainties used in the analysis.

4.2.3 R_{AA} results and comparisons

The R_{AA} plots are produced as described in Sec. A.3.2. See Fig. 18, Fig. 19 and Fig. 20, for examples of points at all centralities shown and for comparison with models and Au+Au results.

4.2.4 Probabilities

Two types of probabilities are calculated: *1)* probability that there is complete suppression of a state, ie. its R_{AA} =0 , and *2)* probability that there is no suppression, ie. $R_{\mathrm{AA}} \geq$1. Since systematics is asymmetric,

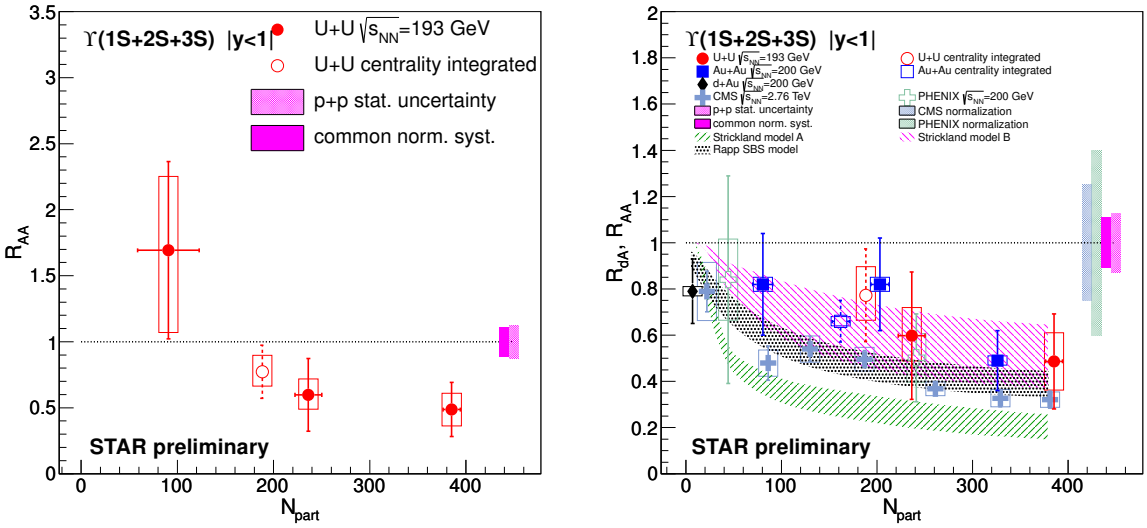

Figure 18: The Υ(1S+2S+3S) $R_{\rm AA}$ versus $N_{\rm part}$, all 3 points (*left*) and significant points compared to d+Au, Au+Au and models (*right*).

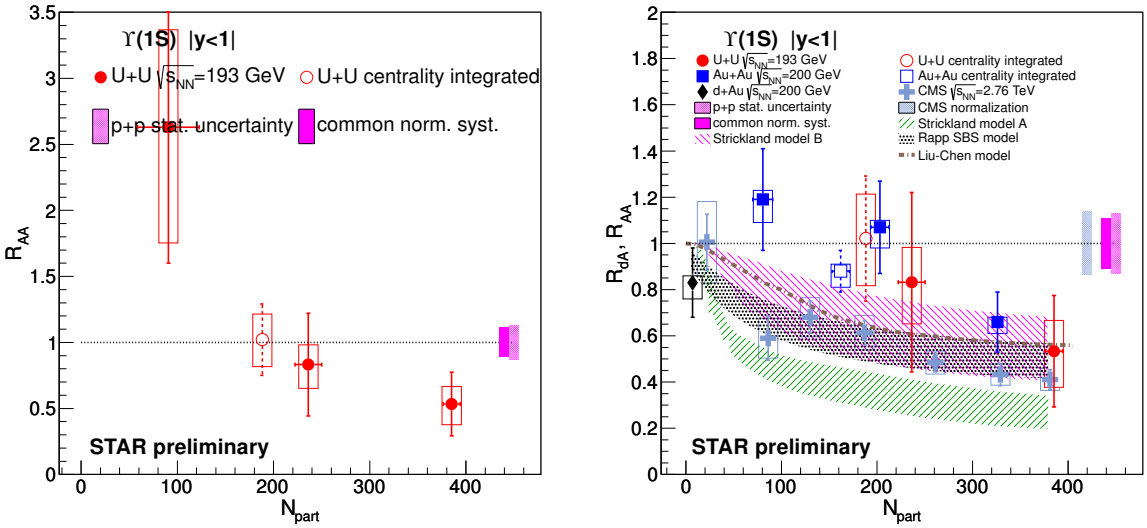

Figure 19: The Υ(1S) $R_{\rm AA}$ versus $N_{\rm part}$, all 3 points (*left*) and significant points compared to d+Au, Au+Au and models (*right*).

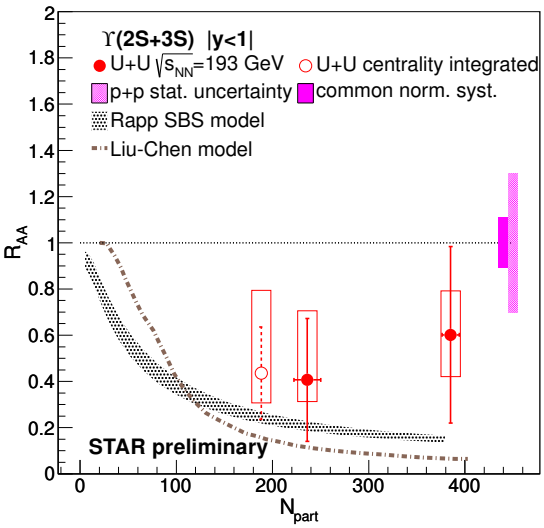

Figure 20: The Υ(1S) $R_{\rm AA}$ versus $N_{\rm part}$ compared to models.

the total distribution is not exactly symmetric. However, the asymmetry is low in most cases, with the exception of the Υ(2S+3S) case. In either case, we suppose that the measured value is above (or below) the actual position in exactly 50% of the cases. Technically, we treat the distributions as Gaussians with the statistical and systematic uncertainties of the respective side summed up quadratically (ie. for $R_{\rm AA}$ $\geq$1, the positive systematic deviation is used). We calculate one-sided probabilities. (that is, the probability of staying within 1-σ is not approx. 0.68 but approx. 0.84.

1. In the case of $R_{\rm AA} = 0$, the distribution is not truncated around zero and not treated as distributions with scarce statistics. This is justified because the background subtraction method allows for fluctuations that cause $R_{\rm AA} < 0$ values. (As it actually happens with the most peripheral Υ(2S+3S) point). Global normalization is not included in the systematics, since that is only a scale factor affecting both counts and error.

2. For $R_{\rm AA} \geq 1$, the global normalization factior (p+p stat. and syst.) are added up quadratically to the systematics.

The combined probability of Υ suppression in Au+Au and U+U is also calculated. This is interesting in the scenario where there is only a weak $R_{\rm AA}(N_{\rm part})$ dependence, since it allows for more pronounced claims. The Best Unbiased Linear Estimate (BLUE) method [20] is used. We employ the simplification that all the systematics in the $R_{\rm AA}$ are 100% correlated between species. This is conservative since it blows up the errors. In most cases it does not matter much since the Au+Au systematics is small compared to its statistical errors. The code is described in Ref. A.4.

A Reconstruction and analysis code

A.1 StL0UpsilonMaker

The code used for finding upsilon candidates in muDST files is a slightly modified version of the code used in the Au+Au analysis. The main Maker is `StL0UpsilonMaker`. It also relies on `StUpsilonCandidate` that defines the tree that will be saved. The `#define USE_REFMULTCORR 0` compiler directive was set (ie. the `StRefMultCorr` class was not used, because it was not ready for U+U by that time. The correction was applied as an afterburner on the next, tree-to-histo level.)

A.2 StUpsilonAnalyzer

The class `StUpsilonAnalyzer` was used to apply the necessary cuts and produce the histograms (in m_{ee}) applying the cuts. It is also capable of producing other output, for efficiency studies etc.. The `StRefMultCorr` [3] class was used on this stage as an afterburner. Since ZDC coincidence rates are stored in the auxiliary `mEventNtuple` but are not directly available in the `ups` tree, a hash-table file `evtable.root`, containing the ZDC coincidence rates for run and event number pairs, is required for this stage. There is an `mEventNtuple.C` class (that has been produced by `TTree::MakeSelector()` and modified accordingly) that can be used to produce this file. See usage within the file.

A.3 Macros

A.3.1 fitUsingRooFit.cxx

The fitting is done with this root macro. Usage is `fitUsingRooFit(const int mult=0, const int idcut=0)` where mult is the selected region ID, and idcut=10 in the current set of analysis cuts.

A.3.2 RAA_UU.C

Drawing and printing $R_{\rm AA}$ results. The macro `RAA_UU.C` is capable of producing different plots, but it needs editing of the main routine `void RAA_UU(int s=0)`. The argument stands for 'state', currently only s=0 meaning Υ(1S+2S+3S) together, and s=1 is Υ(1S). The routine for plotting $R_{\rm AA}$(Npart) is `void plotRaaVsNpart(bool auau=true, bool dau=false, bool all=true, bool drawtheory=true, bool drawcms=false, bool drawphnx=false, bool uu=true, int state=STATE)` .

argument name	true	false
auau	show Au+Au data	show lowest-$N_{\rm part}$ U+U point
dau	show d+Au data	
all	show 0–60% centrality point(s)	
drawtheory	show theory curves	
drawcms	show CMS points	
drawphnx	show PHENIX points	

The legends will be adjusted accordingly. The output is named `plots/Raa_npartXX.eps` for Υ(1S+2S+3S) and `plots1S/Raa1S_npartXX.eps` for Υ(1S), where XX is replaced by a number indexing the argument setup.

Cross sections and errors are printed out by loading the macro and executing `printXsec(int state=0)` where state can be 0 for Υ(1S+2S+3S), 1 for Υ(1S) and 2 for Υ(2S+3S).

The macro can also be used for plotting different figures, eg. `void plotRaaVsPt(int opt=0, int state=STATE)` is for plotting $R_{\rm AA}(p_{\rm T})$, while `void plotXsecVsY(int opt=0, int state=STATE)` and `void plotXsecVsPt(int opt=0, int state=STATE)` plots non-bin-corrected cross sections versus rapidity and $p_{\rm T}$, respectively. These were not used in the analysis.

A.3.3 raa.C and raa3.C

Split-panel $R_{\rm AA}(N_{\rm part})$ plotters for publication-quality plots. raa.C plots Υ(1S+2S+3S) and Υ(1S), raa3.C also adds Υ(2S+3S).

A.3.4 spectrum.C

The macro was used to compute yields in each bin and produce the spectrum plots. First, the raw spectra is corrected for acceptance and efficiency. These are stored/computed in `UpsCrossSections.h`. The errors are also calculated and corrected in a similar way.

A.3.5 binding.C

Macro for plotting $R_{\rm AA}$ versus binding energy. Any uncertainty that is not global normalization but not clearly statistical corresponding to the heavy ion measurement, is included into the systematics error bars (For the Υ points this is p+p statistical uncertainty, which is dependent on which state we are looking at.)

A.4 The BLUE code

The code of Ref. [21], version 2.1.0 was used to compute the correlated unification of $R_{\rm AA}$ values and errors. The module name is `B_Upsilon` (ie. the input files and the code to compile are `B_Upsilon.inp` and `B_Upsilon.cxx` respectively). Type `make`, then run `./BlueOne B_Upsilon`. Note that the code requires `UpsCrossSections.h` which should be properly included.

A.5 The p+p reference code

The code for calculating the $d\sigma_\Upsilon/dy$ dependence on $\sqrt{s}$ is `fitppupsxsec.C`. It uses `xyscan_UpsCrossSec.txt` `xyscan_NLO_CEM.txt` and for the measurements listed in Fig. 9 of Ref. [14] , and for the NLO CEM model from the same location, respectively. (These files were obtained by xyscan, which is one of the the dominating factors in the error of our method, but still negligible.)

B Embedding

Embedding is used to establish most of the acceptance and efficiency corrections as well as for systematic studies, detailed in later sections.

B.1 Code

The embedding request [17] was made with the following parameters: From each state Υ(1S), Υ(2S) and Υ(3S), 25k events were embedded into $\sqrt{s_{NN}} = 193$ GeV U+U data. One $\Upsilon \to {\rm e}^-{\rm e}^+$ was generated flat in $0 < p_{\rm T} < 10$ and in $-1.2 < y < 1.2$, with the same vertex as in the data. For the analysis of the embedding, the same code was used as in the Au+Au analysis [2]. The Maker to run is `StUpsilonEmbedMaker`.

B.1.1 $E_{\rm clus}$ afterburner

An event-by-event $E_{\rm clus}$ correction was applied on the embedding with an afterburner (see Sec. 3.7.3 for details how the correction was established). Correction factors and systematic ranges are calculated when calling the script `dosmear.sh`. This calls `smearupstree.C(char * infile, char * outfile, int params)`, which looks for a simulated `TTree` named `ups` in the file with the name `infile`, appends it with the corrected fields, and saves the new tree in `outfile`. The following new branches are added to the `ups` tree, for the decay positron and electron respectively:

e^+	e^-	meaning
posEoP	eleEoP	uncorrected cluster energy-momentum ratio $E_{\rm clus}^{uncorr}/p$
posEcorr	eleEcorr	corrected cluster energy $E_{\rm clus}^{corr}$
posEoPcorr	eleEoPcorr	corrected cluster energy-momentum ratio $E_{\rm clus}^{corr}/p$

The argument `params` chooses the desired parameter set according to the following:

param	effect
0	"default" = averages of lower and upper means
1	lower limit of means taken
2	upper limit of means taken
3	lower limit of sigmas taken
4	upper limit of sigmas taken
5	applies point-by-point correction

The actual functions to compute smearing are in `SmearUtils.h`.

B.2 Macros

B.2.1 Efficiencies.C

Calculate efficiencies and dumps it in a tabular to the standard output. Uses `Tools.h` where cuts, embedding event weights, input files, Crystal ball shape etc. are defined. It takes two parameters: `state=1` loads the Υ(1S) data file, while 2, 3 and 0 the Υ(2S), Υ(3S) and all merged, respectively. The

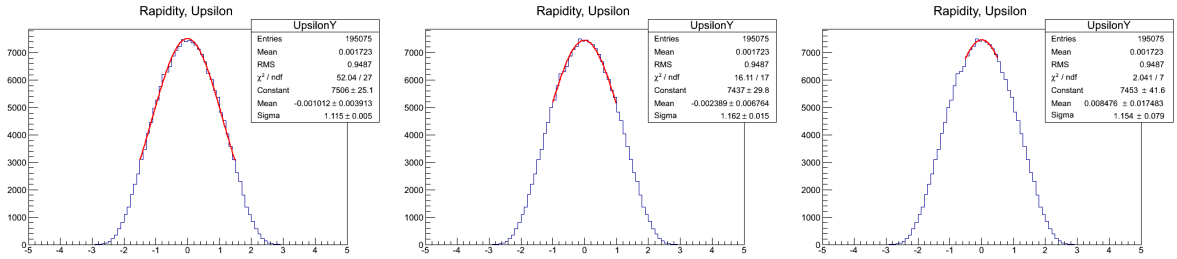

Figure 21: Rapidity distribution from Pythia, fit ranges of $|y| < 1.5$, 1 and 0.5.

other parameter defaults to `style=1` which creates plain text output, while 2 creates latex formatted tabular. For a "stripped" version without a header, use 0.

B.2.2 plotEffs.C

Shows reconstruction efficiencies, listed in Tables 11, 12 and 13, in a visual form. Looks for input files `effs1S.txt`, `effs2S.txt` and `effs3S.txt` containing the efficiencies in a stripped text table format (as from `Efficiencies.C(1,0)` etc.).

B.2.3 SingleEoPeffs.C

This macro calculates efficiencies of the $Eclus/p$ cut, with respect to p, with a binning, start point, end point (optionally a moving dp-window size if desired to be different from the step size), specified as arguments in such order.[6]

B.2.4 plotSingle.C

Simple plotter for single electron efficiency distributions using hardwired values, copied from the output above. Input file containing efficiency factors and their errors can be specified as an input file. The standard output dumped out by `SingleEoPeffs.C` can be used right away.

B.3 p_{T}- and y-weighting of embedding

The embedded samples come flat in y and p_{T}. The p_{T} weighting was done according to the slope $T = a\ln(\sqrt{s_{\mathrm{NN}}} + b)$, where $a = 0.45$ and $b = -1.23$ as determined in [2] yields T=1.16 GeV. The slope of the measured spectrum is consistent with this value, see 4.1).

The rapidity distribution was determined using Pythia. Fig 21 shows the obtained distribution with a wide ($|y| < 1.5$), middle ($|y| < 1$) and narrow range ($|y| < 0.5$) fit. These yield $\sigma = 1.10, 1.16$ and 1.15 respectively. Since the edge of distribution is lost because of acceptance, and y>1 hits do not play much role, $\sigma = 1.15$ was taken for weighting the embedding.

The resulting efficiencies are listed in Table 14.

B.4 Mass peak fits

The mass peaks are parametrized in order to get templates to use in the data peak fitting. Crystall Ball fits are shown in Fig. 22. The parameters are summarized in Table 17. Fits to the corrected Υ spectra are consistent with this value within its errors.

[6] Since the distribution in p of the decay electrons is uneven, a weighting might be used is applied that restores an approximately flat p-distribution of single electrons. The following function, applied reciprocially as weights to simulated hits, was obtained by simple fits to the distribution shown in the 1st panel of Fig. 23 .

$$1/w(p) = \begin{cases} -105.5 - 488.1p + 596.8p^2 - 74.96p^3, & \text{if } p < 5 \text{ GeV}/c \\ \exp(-0.1839p), & \text{if } p \geq 5 \text{ GeV}/c \end{cases}$$

The effect of the weighting in the resulting efficiency values, however, is usually less than a percent even in the case of 1 GeV/c bin sizes, so this option was commented out when using the macro for analysis.

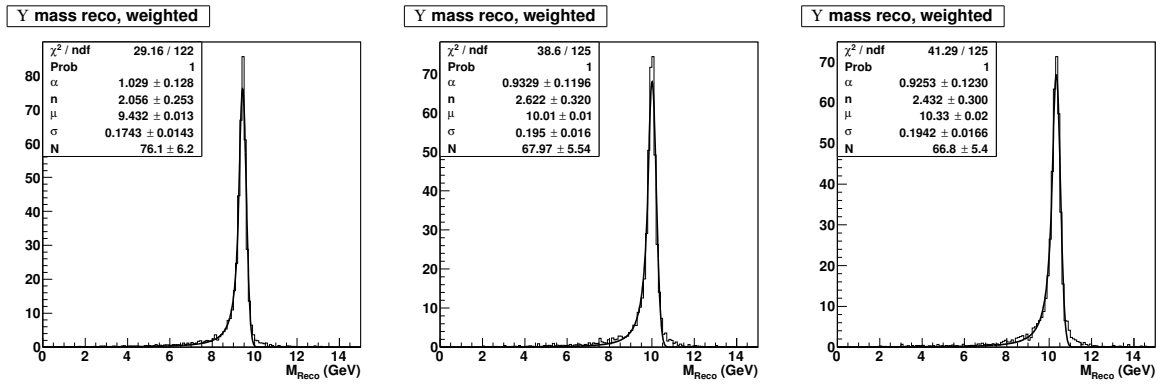

Figure 22: Υ(1S), Υ(2S) and Υ(3S) mass peaks after p_{T} and y-weighting of events. The fits are Crystal ball functions, with parameters summarized in Table 17.

state	α	n	μ	σ
Υ(1S)	1.19924	1.49488	9.42715	0.192990
Υ(2S)	1.14317	1.64211	9.99365	0.211215
Υ(3S)	1.14309	1.66457	10.3176	0.218668

Table 17: Parameters of the Crystal ball fits. Note that the normalization parameter N is not listed. The ratio of states measured from p+p is $\Upsilon(1S) : \Upsilon(2S) : \Upsilon(3S) = 157.1 : 41.6 : 28.8$.

B.5 Momentum-weight factors

In several cases the efficiency/correction factors are obtained in momentum bins, and have to be weighted according to the real distribution of Υ decay electrons (triggered, paired, any...).

Fig. 23 and Fig. 24 shows the distribution of Υ(1S) decay electrons in each momentum and transverse momentum bin respectively.

The p-weighting was done using the macro `weigh.C` for the following quantities:

- `void weigh_Guannan_nSigE_eff()` : Compute and print $n\sigma_{\mathrm{e}}$ efficiencies and errors from p_{T} bins based on photonic sample
- `void weigh_nSigE_eff()` : Compute and print $n\sigma_{\mathrm{e}}$ efficiencies from p bins based on TPC-identified electrons
- `void weigh_EoP_eff_trig()`: Compute and print $Eclus/p$ triggered cut efficiencies (data, embedding, ratio, errors) on the triggered particle from p bins
- `void weigh_EoP_eff_pair()`: Compute and print $Eclus/p$ paired cut efficiencies (data, embedding, ratio, errors) on the paired particle from p bins
- `void weigh_Match_eff()`: Compute and print matching efficiencies (embedding, data, ratio) from p bins

C Identified electron datasets

C.1 Electron candidate tracks

The `StTrackSampleMaker` was used over NPE18 triggered data to collect pre-selected electron candidates, with good quality $p > 0.5$ GeV/c tracks coming from the primary vertex, matched to a BEMC cluster in a similar way to the StUpsilonMaker, and saved into a TTree called `singleTrack`, defined in `StSingleTrack`. This results in a fairly large data sample size, altogether 23 GB in three aggregated files (singleTracks-[SUM,SUM_1,SUM2].root). The cuts on $n\sigma_{\mathrm{e}}$, compactness, matching (R_{SMD}) etc. were than applied on the sample on analysis level.

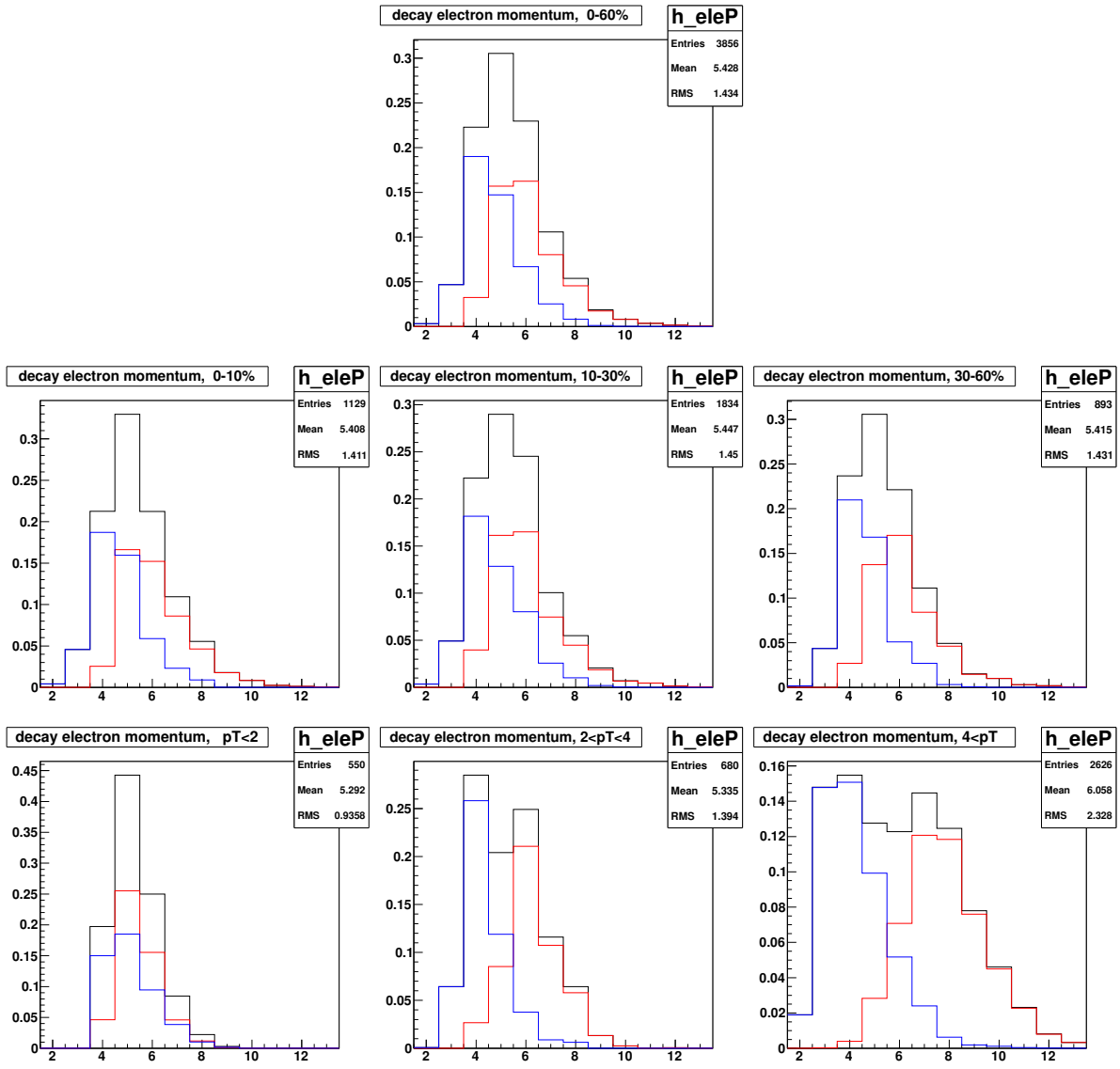

Figure 23: Momentum (p) weights of triggered (red), paired (blue) and all clusters (black). Top: All data in 0-60% centrality. Second row left to right: 0-10%, 10-30% and 30-60% centralities; Third row left to right: $0< p_{\mathrm{T}} < 2$ GeV/c, $2< p_{\mathrm{T}} < 4$ GeV/c, $4< p_{\mathrm{T}} < 10$ GeV/c, respectively.

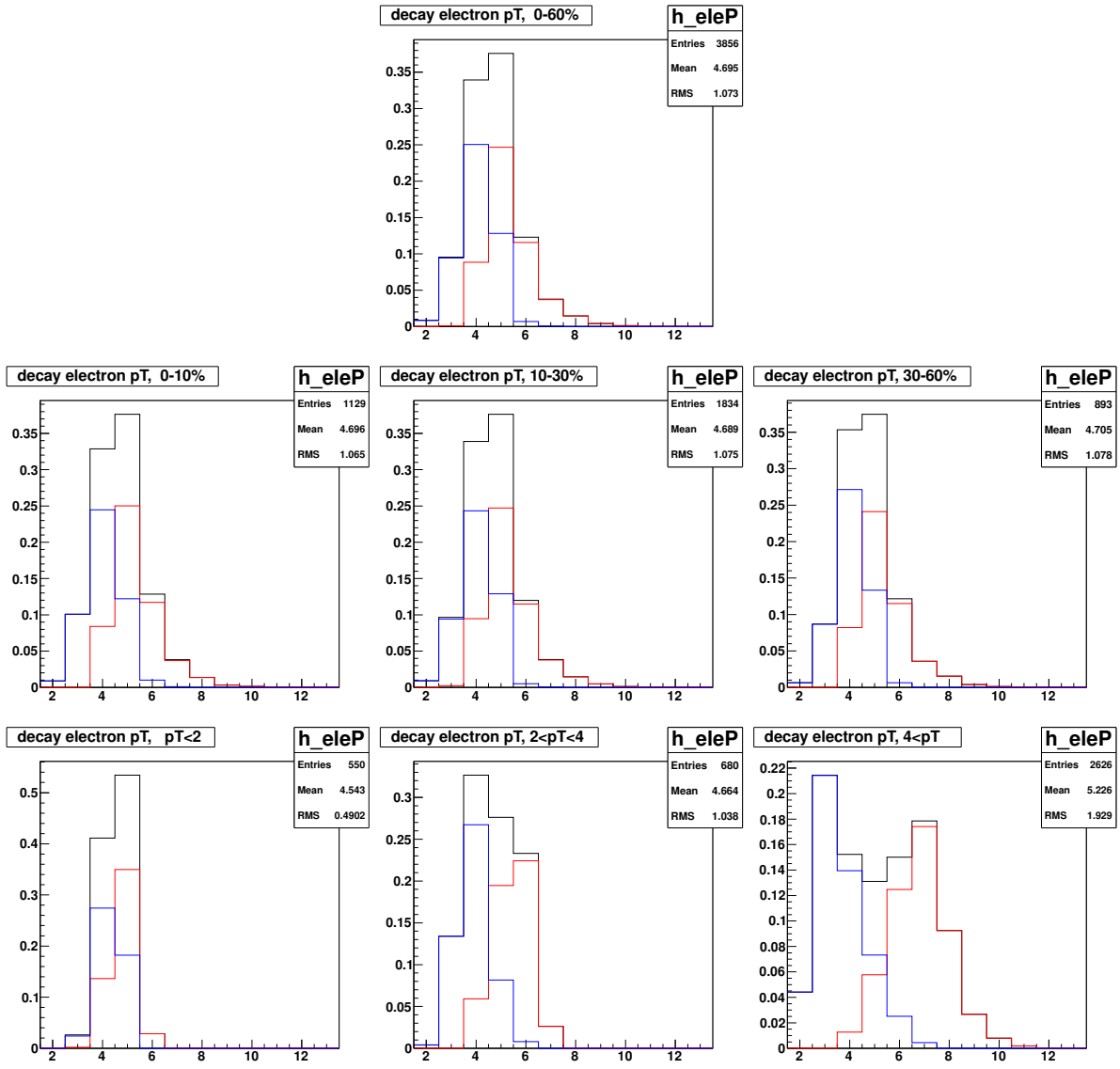

Figure 24: Transverse momentum (p_{T}) weights of triggered (red), paired (blue) and all clusters (black). Top: All data in 0-60% centrality. Second row left to right: 0-10%, 10-30% and 30-60% centralities; Third row left to right: $0< p_{\mathrm{T}} < 2$ GeV/c, $2< p_{\mathrm{T}} < 4$ GeV/c, $4< p_{\mathrm{T}} < 10$ GeV/c, respectively.

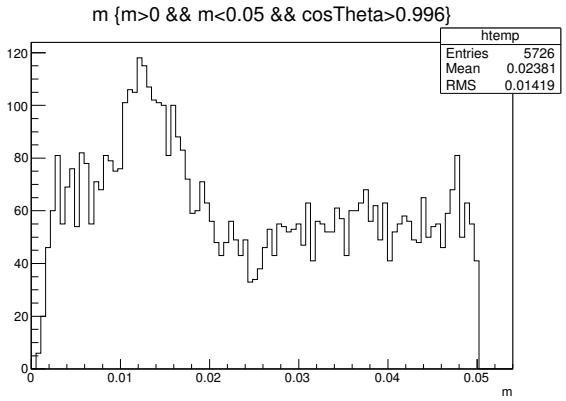

Figure 25: Sample photonic enhanced cut. The photonic peak is clearly visible and dominant below $m = 0.02$ GeV/c^2

C.2 TPC, EMC and photonic-enhanced samples

In order to decrease sample size, a similar maker `StTrackConvEleMaker` was utilized, that carries out certain preselections. A simplified reconstruction of a paired electron was also added in this code, in order to produce a photonic electron enhanced sample. The data size (aggregated file `eleCand-SUM.root`)) was reduced to a single ile of 1.5 GB.

- **TPC-identification** : The candidate had to fulfil the additional $n\sigma_{\rm e} > 0.5$ track electronness condition in order to be saved to the `tpcele` tree.
- **EMC-identification** : The candidate had to fulfil $0.8 < E_{\rm clus}/p < 1.35$ in order to be saved to the TTree `emcele`. One candidate may have been saved to both trees.
- **Photonic-enhanced** : In the case an electron-like pair was found with $-1.5 < n\sigma_{\rm e} < 3$ and $E_{\rm tower}/p > 0.2$, the invariant mass m was calculated. A further variable $pairFlag$ indicates other conditions that the pair fulfils, the smaller the more photonic-like. A $pairFlag = 0$ is credited if $0.8 < E_{\rm clus}/p < 1.35$, $m < 0.02$ and the opening angle is $cos(\vartheta) > 0.9998$. If there are more pairs, the one that comes with the smallest $pairFlag$ is saved.

Fig. 25 shows the pair m distribution for photonic-like electrons with $cos(\vartheta) > 0.996$, the cut used in analysis together with an $m < 0.02$.

C.3 Electrons from J/ψ decays

The identified electrons from decays of J/ψ were obtained with `StMBJpsiMaker`, a maker derived from `StL0UpsilonMaker`. The main differences are that Minimum Bias trigger is used, however, the NPE11 condition is applied in the maker to reduce statistics from low-momentum pairs. A "triggered" electron candidate (to be used in the analysis) has to fulfil only loose ID cuts ($p > 1$ GeV/c, $E_{\rm clus}/p < 3$ on top of usual quality cuts), however, the pair is required to be strongly electron-like ($0.75 < E_{\rm clus}/p < 1.40$, $E_{\rm tower}/E_{\rm clus} > 0.5$). The reconstructed invariant mass has to fall into the window $2.9 < m < 3.2$. Both like- and unlike-sign pairs are reconstructed to allow for analysis-level background subtraction. These cuts provided very few candidates after background subtraction, especially in higher $p_{\rm T}$ bins, therefore the J/ψ sample was mostly used as a cross-check besides other samples.

C.4 TPC $n\sigma_{\rm e}$ fits

The macro `sigma_eff.C` was used to establish $n\sigma_{\rm e}$ fits on single identified tracks. Cuts at $R_{SMD} < 0.4$, $E_{\rm tower}/E_{\rm clus} > 0.8$, $0.8 < E_{\rm clus}/p < 1.3$, $ADC > 180$ were applied. Two different ways were used, yielding similar result for the electrons.

1. Three Gaussians were fitted to represent the pion, kaon and electron peak.

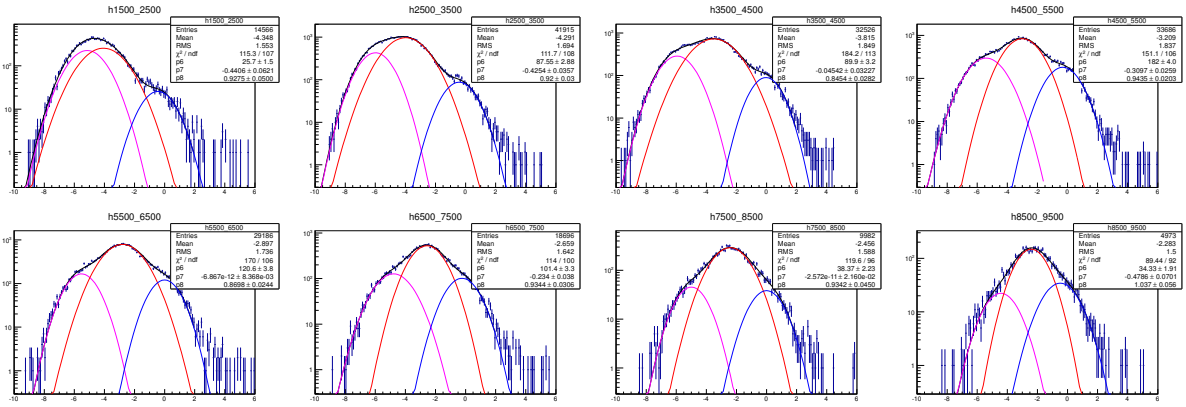

Figure 26: Single-track $n\sigma_e$ distributions fitted with 3 Gaussians for one-GeV/c momentum bins from p=2 GeV/c up to p=9 GeV/c.

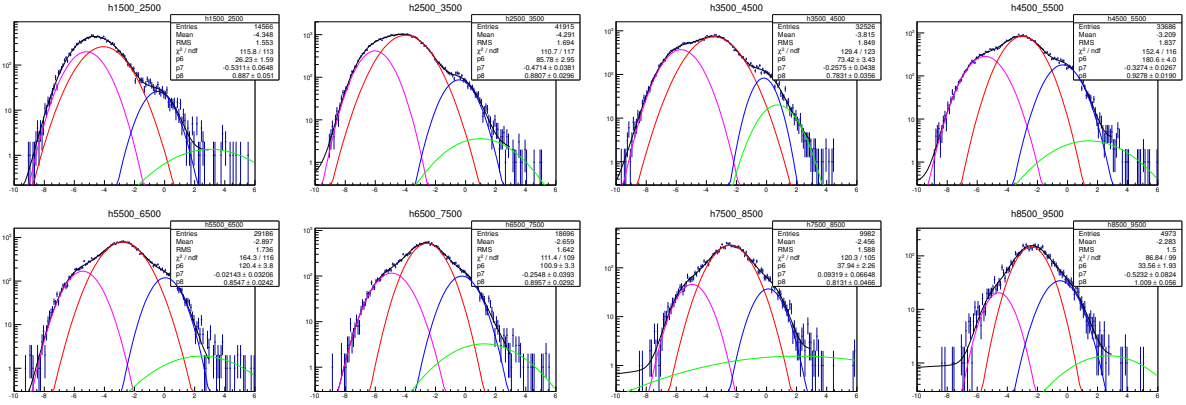

Figure 27: Single-track $n\sigma_e$ distributions fitted with 4 Gaussians for one-GeV/c momentum bins from p=2 GeV/c up to p=9 GeV/c.

2. A fourth Gaussian was added with free parameters, to account for any instability / non-Gaussianity. (Mostly for merged pions).

Results are listed in Figs. 26 and 27 respectively.

C.5 Photonic electrons

In the NPE18 U+U→ J/ψ+X analysis, photonic electrons were used to calculate the efficiencies [15]. After photonic electron reconstruction and background subtraction, the $n\sigma_e$ distributions were fitted with gaussians in several p_T slices. The same fit results were used in this analysis, among different methods. Fig. 28 is a screenshot of slide 12 of Ref. [15], showing fits and fitted electron distribution parameters for several of the p_T bins.

D Verification of simulation with data

The main routines are in `simver.h`. The routine `void simver()` shows examples of usage.

D.1 Matching

The matching parameter $R = \sqrt{(\Delta\eta)^2 + (\Delta\varphi)^2}$ is investigated in 1 GeV/c wide p_T bins. Identified electrons identification cuts are compared to embedding in Fig 29, photonic-enhanced electrons to em-

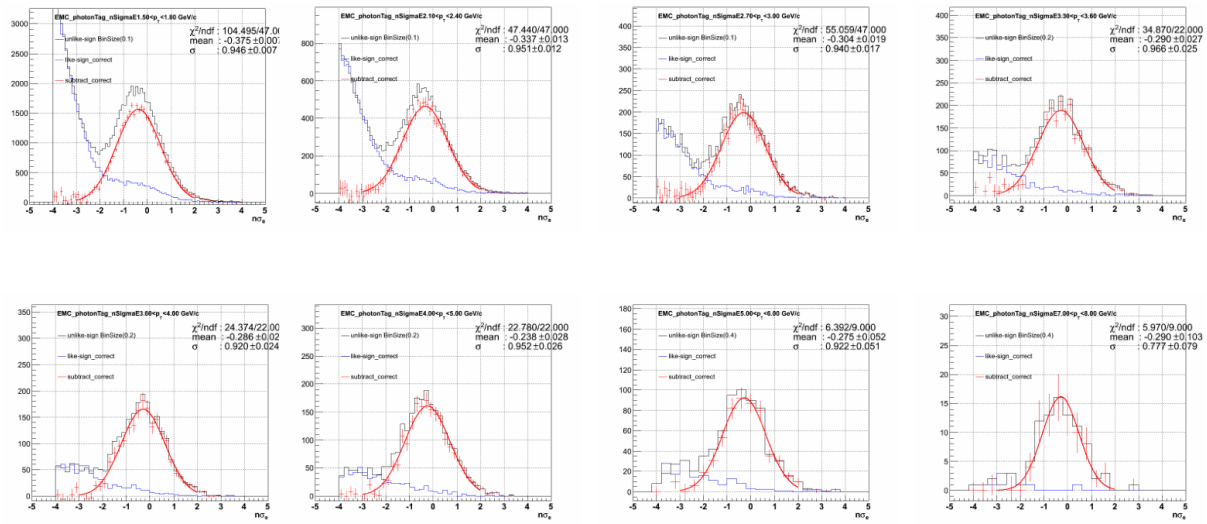

Figure 28: Distributions of photonic electron $n\sigma_e$ fitted, with fit parameters listed in several p_T bins.

bedding in Fig 30. The former sample suffers from large contamination in the lower bins, while statistics gets scarce in higher bins for the latter.

D.2 E_{clus}/p

Figure 31 shows examples of the E_{clus}/p distribution of identified electron sample compared to embedded simulations, within the $5 < p < 6$ GeV/c range. Both samples show that data is not reproduced well with embedding. Although the triggered sample may be biased especially at lower momentum bins, photonic electrons show a remarkably similar distribution.

Therefore a more through investigation was necessary in order to establish corrections. The E_{clus}/p distributions were recorded in 8, 1 GeV/c wide momentum bins starting from bin 2.5-3.5 GeV/c. Figs. 32 and 33 show the distributions of E_{clus}/p for embedding, single TPC-identified and photonic-enhanced electron samples, respectively.

The fit parameters are shown in Fig. 12. An event-by-event correction on the embedding is determined by parametrizing embedding and data fit parameter dependences on the momentum, as described in Section 3.7.2. The corrected embedding is compared to the uncorrected one on Fig. 34. The resulting single electron efficiencies are shown in Fig. 13.

D.3 E_{tower}/E_{clus}

Examples of compactness distributions for the triggered particles are shown in Figs. 35, 36 from single identified electrons and triggered Υ candidate samples, trigger conditions required in both cases.

D.4 ADC

D.5 adc0 vs. E_{tower}

The verification of ADC cut is done in narrow E bins (that has to be narrow enough that the biased E distribution does not shift the means too much). When using NPE18 triggered data, the 3-6 GeV range is also strongly influenced by trigger turn-on. Therefore in the lowest range, background-subtracted J/ψ decay electrons were used. These sample plots are shown in Fig 37.

D.6 dsmADC vs. adc0

In order to understand the trigger turn-on around dsmADC=18, the J/ψ sample was used. The ADC0 distributions for each dsmADC value are plotted in Fig. 38. The Gaussian fit parameters are shown in

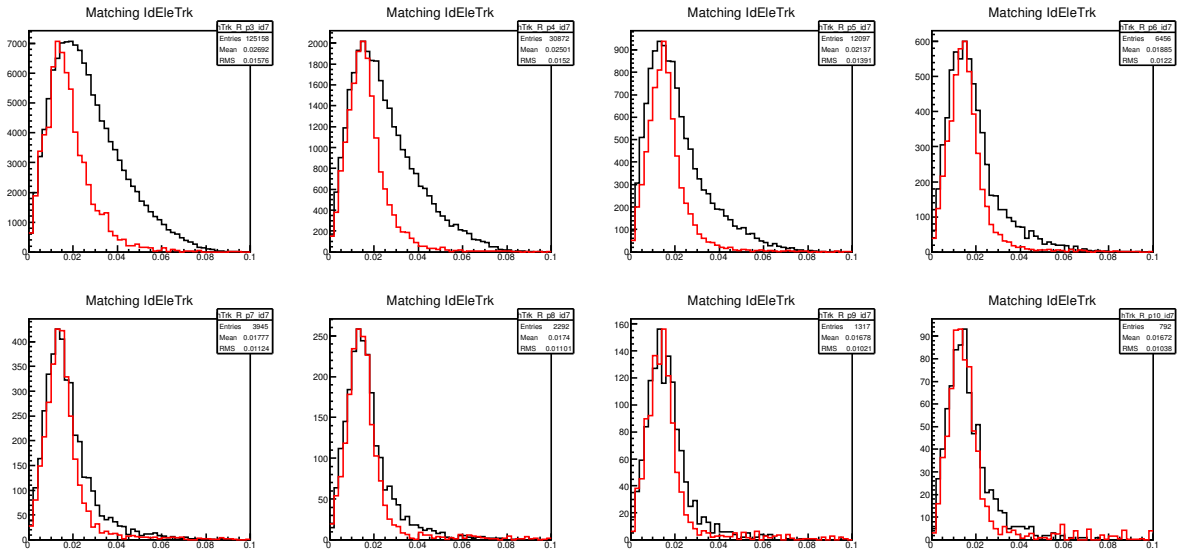

Figure 29: Matching parameter R for identified electrons in 1 GeV/c wide momentum bins. ID cuts were $|n\sigma_{\mathrm{e}}| < 3$, $|n\sigma_{\pi}| > 2$, $0.9 < E_{\mathrm{clus}}/p < 1.4$, $E_{\mathrm{tower}}/E_{\mathrm{clus}} > 0.8$ for data. Only the calorimeter cuts are applied for embedding.

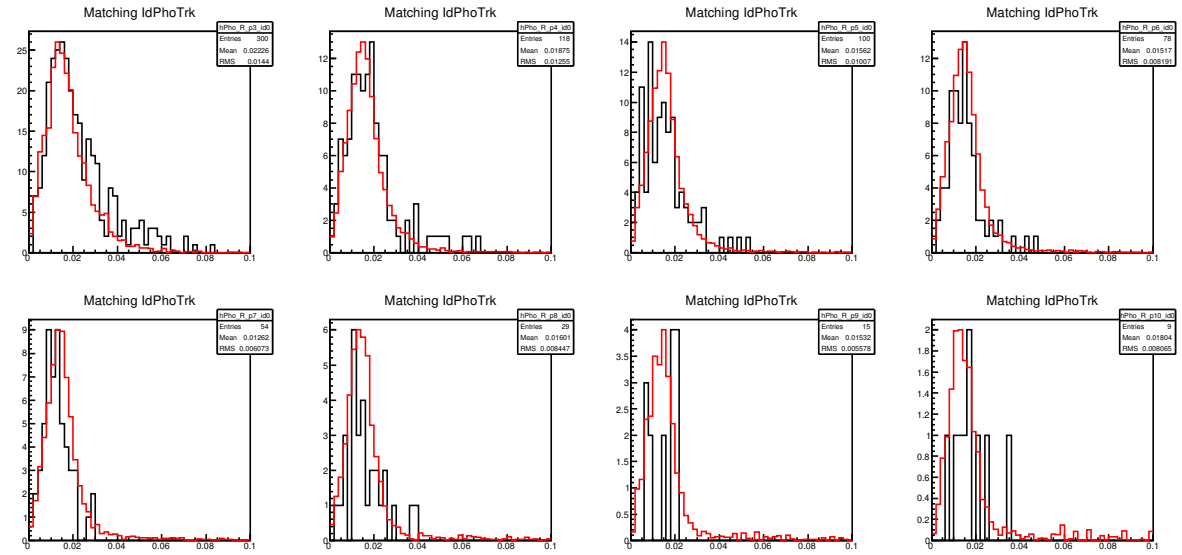

Figure 30: Matching parameter R for photonic-enhanced electrons in 1 GeV/c wide momentum bins. The $M < 0.02$ GeV photonic cut was applied for data.

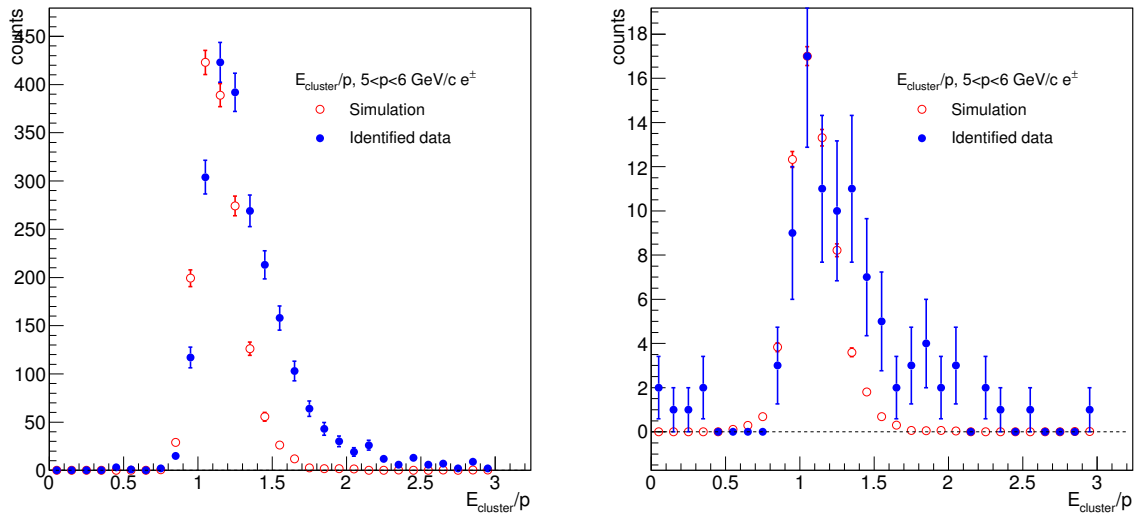

Figure 31: Example E_{clus}/p distribution of identified electron samples compared to embedded simulations, at $5 < p < 6$ GeV/c. On the left side, L0-triggered sample is compared to simulations with an ADC>297 condition applied, together with strong identification conditions in the TPC ($|n\sigma_{\mathrm{e}}| < 3$ and $|n\sigma_{\pi}| > 2$). On the right side, photonic-enhanced samples compared to embedding within detector acceptance.

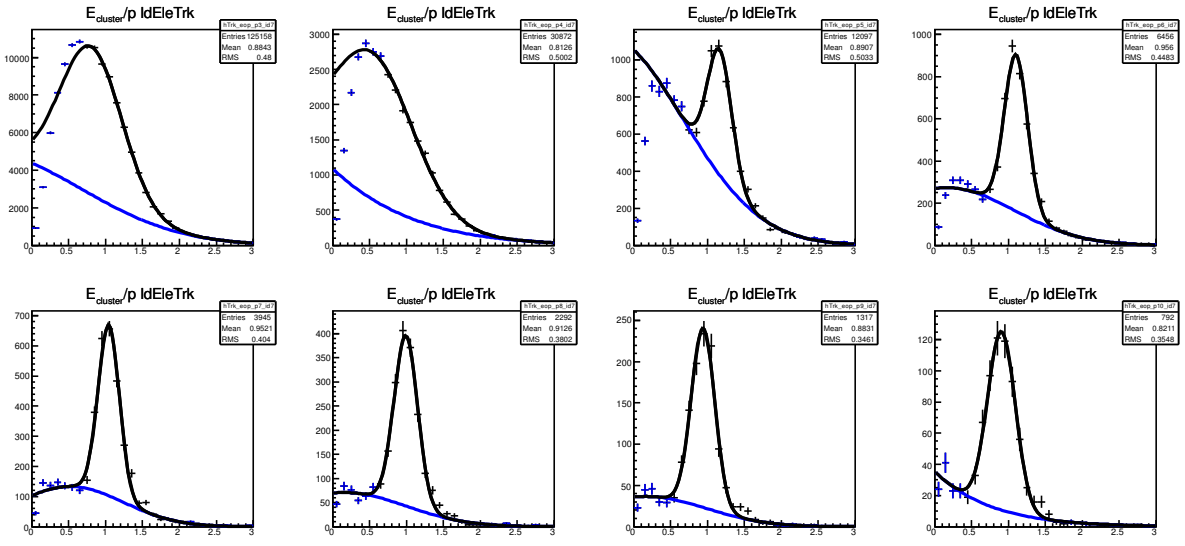

Figure 32: Identified electron E_{clus}/p distributions (black crosses) in 1 GeV/c momentum bins, after TPC cuts $|n\sigma_{\mathrm{e}}| < 3$ and $|n\sigma_{\pi}| > 2$. The background is fitted as a Gaussian on an appropriately determined sideband (blue crosses). The peak is fitted as a Gaussian on top of the background. Note that the fit fails due to the huge background in the 1st two bins.

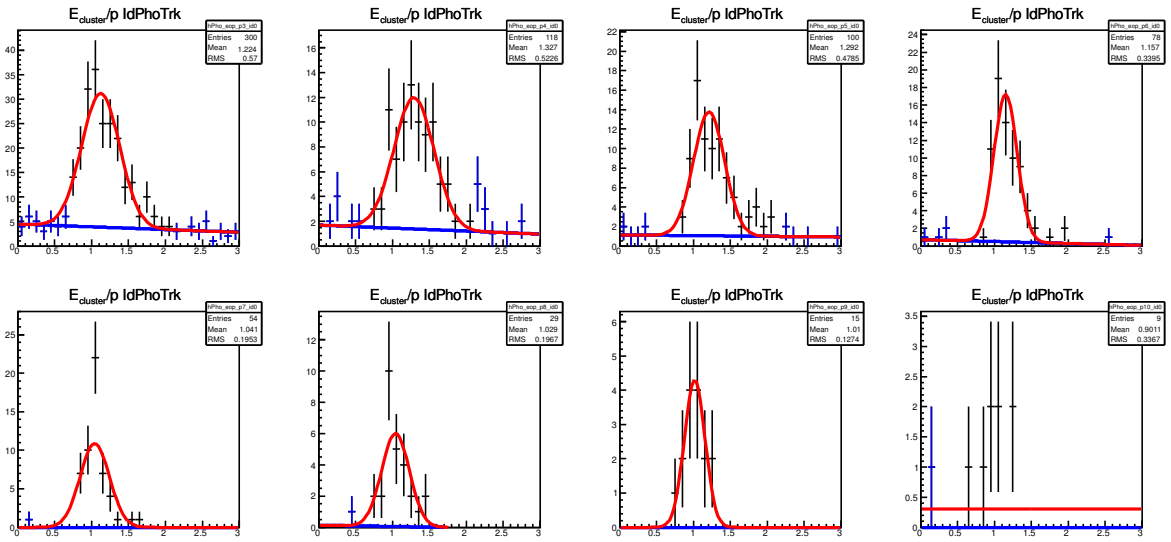

Figure 33: Photonic-enhanced electron E_{clus}/p distributions (black crosses) in 1 GeV/c momentum bins, after TPC preselection cuts and an m<0.2 GeV cut. The background is fitted as a linear fit using the likelihood method on an appropriately determined sideband (blue crosses), unless there is at least one hit in each side, in which case the background is considered zero. The peak is fitted as a Gaussian on top of the background. Note that the fit fails in the last bin.

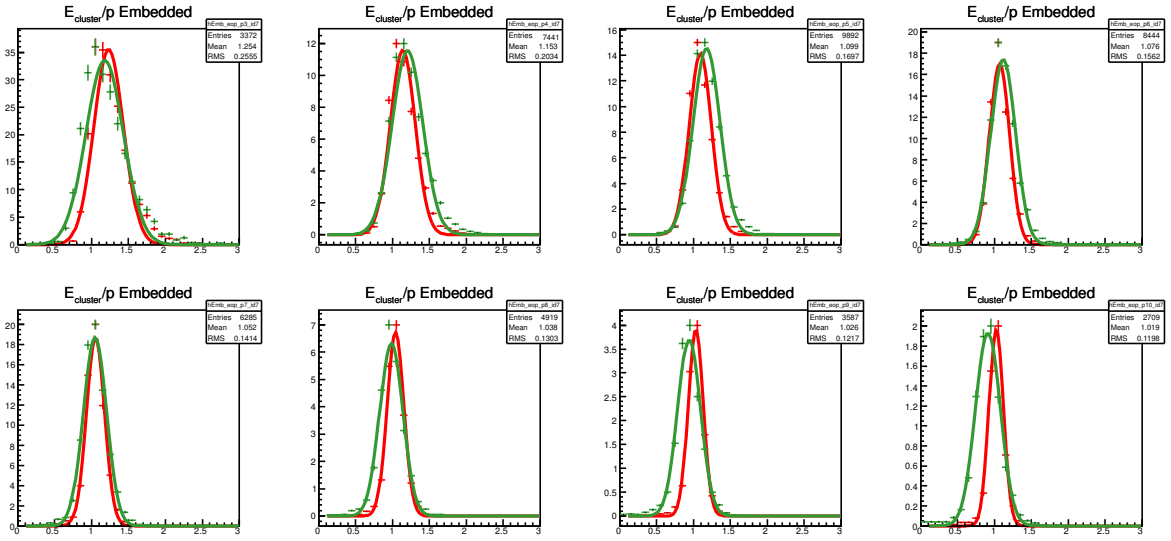

Figure 34: Uncorrected (red) and corrected (green) E_{clus}/p distributions from embedding in 1 GeV/c momentum bins. The peaks are fitted with a Gaussian.

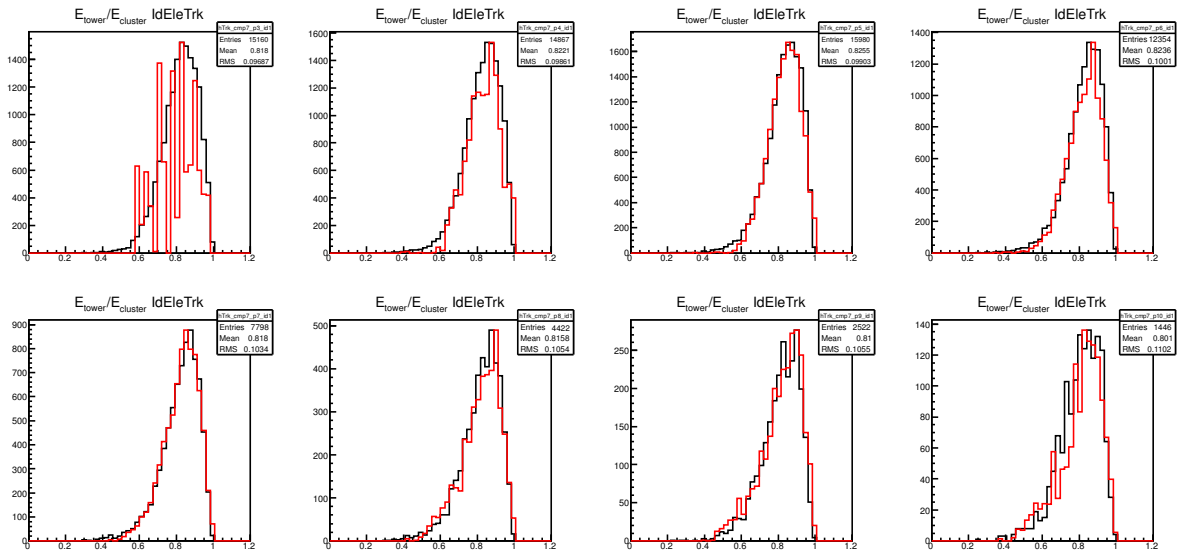

Figure 35: Compactness parameter $E_{\text{tower}}/E_{\text{clus}}$ for identified electrons in 1 GeV/c wide momentum bins. ID cuts were $|n\sigma_{\text{e}}| < 3$, $|n\sigma_{\pi}| > 2$, $0.75 < E_{\text{clus}}/p < 1.45$, with trigger conditions applied. Only the trigger condition and calorimeter cuts are applied for embedding.

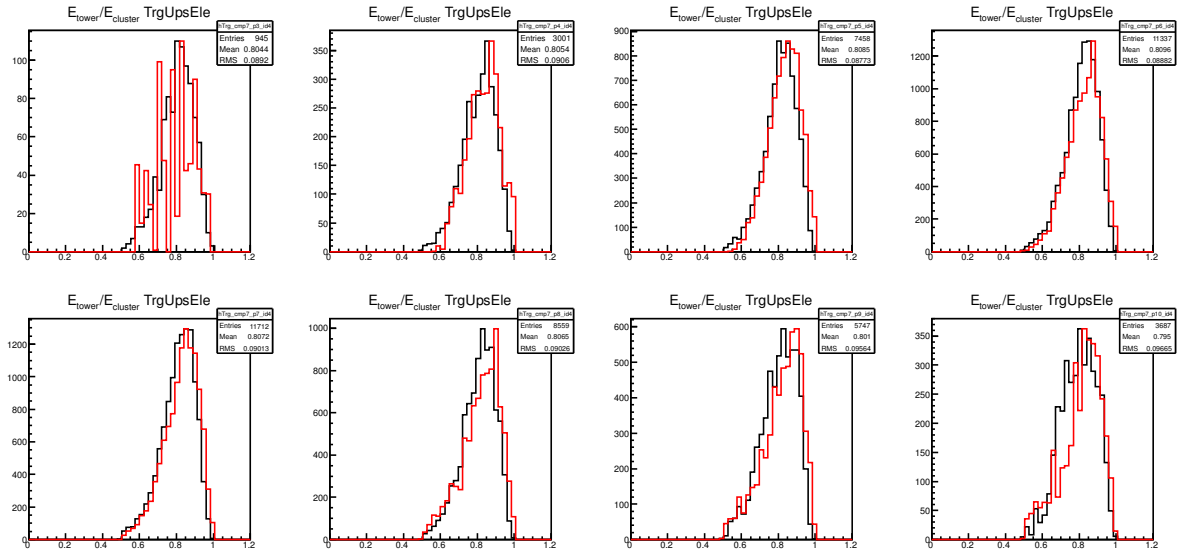

Figure 36: Compactness parameter $E_{\text{tower}}/E_{\text{clus}}$ for triggered electrons of Υ candidates, in 1 GeV/c wide momentum bins. ID cuts were $|n\sigma_{\text{e}}| < 3$, $|n\sigma_{\pi}| > 2$, $0.5 < E_{\text{tower}}/E_{\text{clus}}$. Only the trigger condition and calorimeter cuts are applied for embedding.

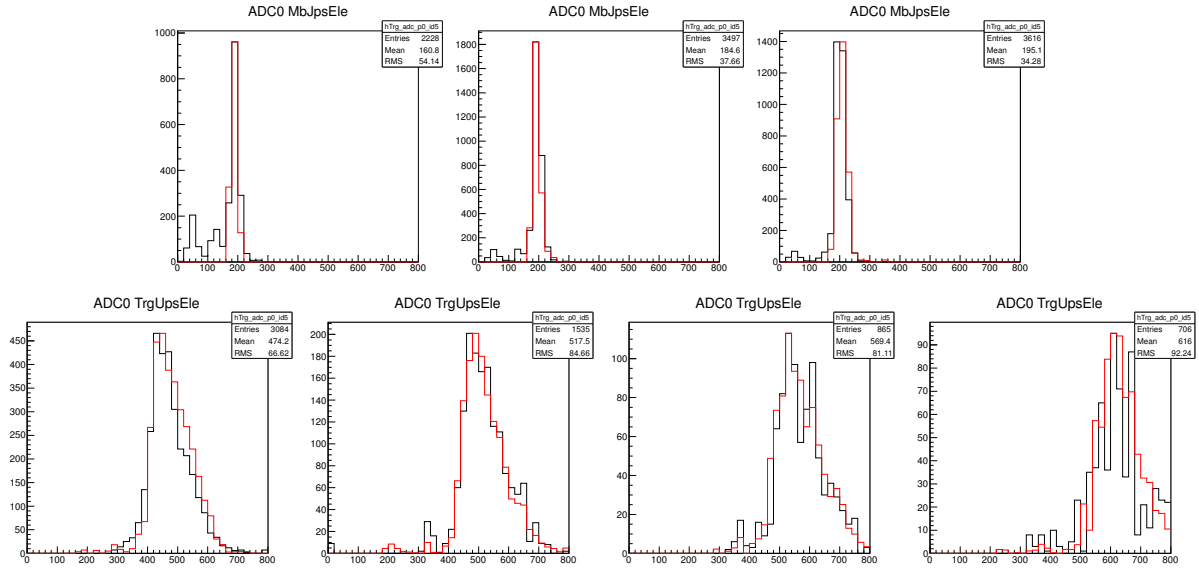

Figure 37: ADC turnon curve in relatively narrow energy bins. Top row: Background-subtracted J/ψ decay electrons with $E_{\rm tower}/Eclus$>0.5, NPE11 condition (data) and ADC>176 (simulation) applied. Energies are 2.20<E<2.30 GeV, 2.45<E<2.55 GeV, 2.70<E<2.80 GeV respectively. Bottom row: Υ decay triggered electrons, NPE18 condition (data) and ADC>303 (simulation), $E_{\rm tower}/Eclus$>0.5 condition applied. Energies are 8<E<9 GeV, 9<E<10 GeV, 10<E<11 GeV and 11<R<13 GeV respectively.

Fig. 39 from dsmADC=15 to 25. The means are parametrized with a linear fit, with the intercept being small. A linear fit on sigmas yield a virtually constant $\sigma = 9$ value over the whole dsmADC range.

References

[1] L. Adamczyk *et al.* [STAR Collaboration], "Suppression of Upsilon Production in d+Au and Au+Au Collisions at $\sqrt{s_{NN}} = 200$," Phys. Lett. B **735**, 127 (2014) [arXiv:1312.3675 [nucl-ex]].

[2] M. Calderón, A. Kesich, "On the Υ analysis of $\sqrt{s_{NN}} = 200$ GeV p+p, d+Au and Au+Au collisions in STAR", `https://drupal.star.bnl.gov/STAR/pwg/heavy-flavor/upsilon-analysis/upsilon-paper-pp-dau-auau/upsilon-pp-dau-auau-paper-documents`

[3] H. Masui, `CVS:offline/users/hmasui/StRefMultCorr`

[4] H. Masui, `http://www.star.bnl.gov/protected/bulkcorr/hmasui/2013/Centrality_UU_193GeV/hmasui_centrality_UU_200GeV_bulkcorr_Mar20_2013.pdf`

[5] `https://drupal.star.bnl.gov/STAR/blog/yezhenyu/nbinary-and-npart-uu-collisions-zhenyu`

[6] `https://root.cern.ch/drupal/content/roofit`

[7] `https://drupal.star.bnl.gov/STAR/blog/rvertesi/2013/nov/21/upsilon-1s-2s-3s-embedding-qa`
`https://drupal.star.bnl.gov/STAR/system/files/Ups1SEmbeddingQA.pdf`

[8] `https://drupal.star.bnl.gov/STAR/system/files/UpsSystematics11b.pdf`

[9] `https://drupal.star.bnl.gov/STAR/system/files/Upsilon12_simufit.pdf`

[10] M. Calderón, `https://drupal.star.bnl.gov/STAR/pwg/heavy-flavor/upsilon-analysis/estimating-drell-yan-contribution-nlo-calculation`

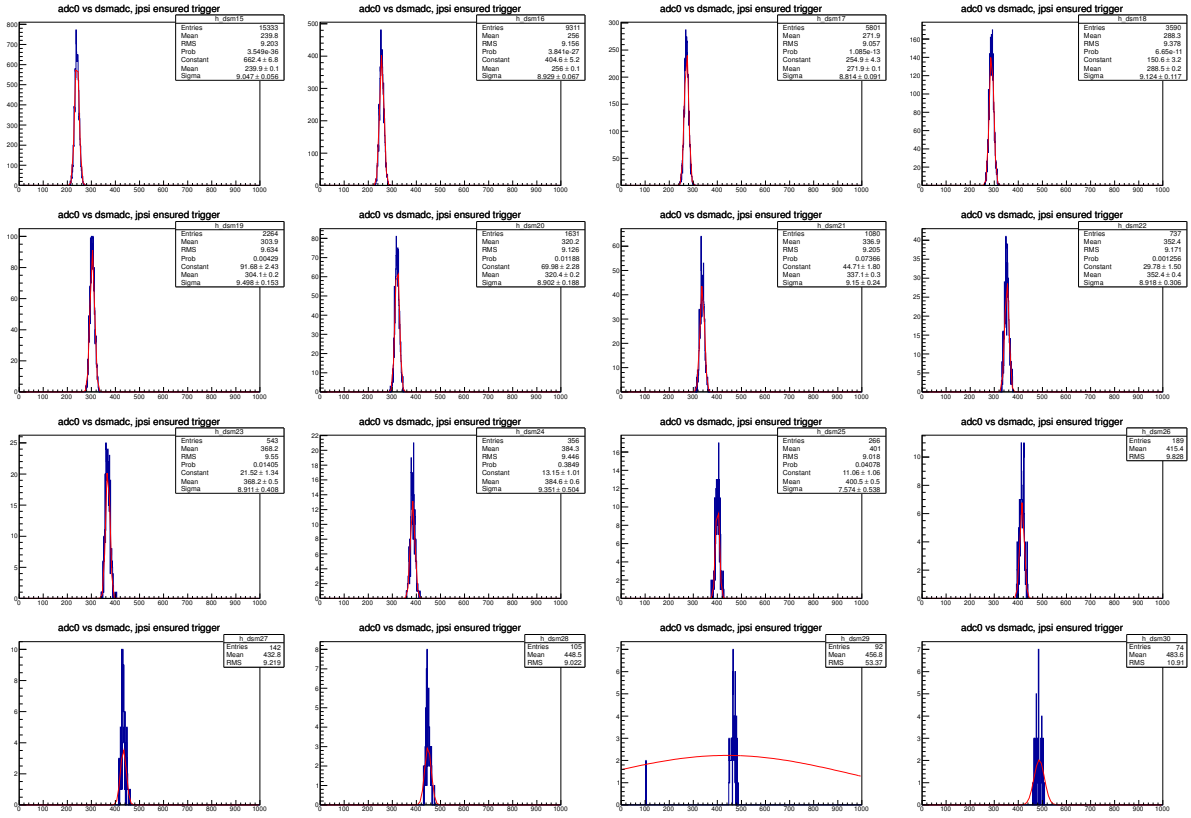

Figure 38: ADC distributions for each dsmADC value: left to right, top to bottom, starting from dsmADC=15

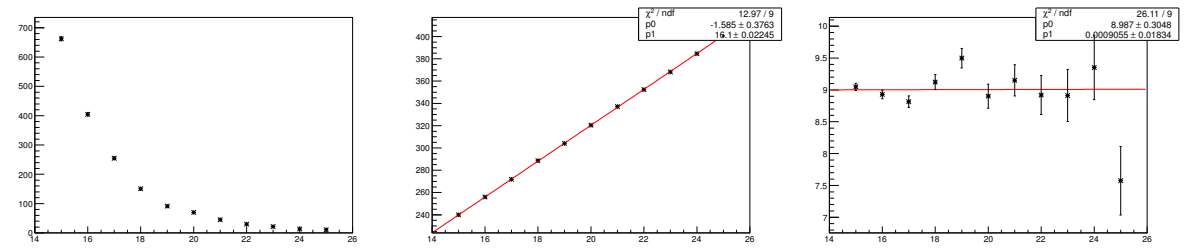

Figure 39: Constants (left), means (mid) and sigmas (right) of ADC distribution gaussian fits versus dsmADC.

[11] M. Calderón, https://drupal.star.bnl.gov/STAR/pwg/heavy-flavor/upsilon-analysis/using-pythia-8-get-b-bbar-ee

[12] G. A. Schuler and T. Sjostrand, "Hadronic diffractive cross-sections and the rise of the total cross-section," Phys. Rev. D **49**, 2257 (1994).

[13] M. M. Block and F. Halzen, "Forward hadronic scattering at 7 TeV: Predictions for the LHC: An Update," Phys. Rev. D **83**, 077901 (2011) [arXiv:1102.3163 [hep-ph]].

[14] M. Bedjidian *et al.*, "Hard probes in heavy ion collisions at the LHC: Heavy flavor physics," hep-ph/0311048.

[15] G. Xie, Z. Tang, "J/ψ in U+U collisions with HT trigger", https://drupal.star.bnl.gov/STAR/meetings/star-collaboration-meeting-spring-2014/heavy-flavor-pwg-session-i/jpsi-uu-collisions-with-ht-trigger

[16] O. Kukral, "J/ψ in U+U analysis status" (9 Jan .2014) , https://drupal.star.bnl.gov/STAR/system/files/KukralHFJanuary.pdf

[17] https://drupal.star.bnl.gov/STAR/starsimrequests/2013/aug/22/upsilon-uu-193-gev-run-12

[18] H. Masui, B. Mohanty and N. Xu, "Predictions of elliptic flow and nuclear modification factor from 200 GeV U + U collisions at RHIC," Phys. Lett. B **679**, 440 (2009) [arXiv:0907.0202 [nucl-th]].

[19] B. Alver, M. Baker, C. Loizides and P. Steinberg, "The PHOBOS Glauber Monte Carlo," arXiv:0805.4411 [nucl-ex].

[20] A. Valassi, "Combining correlated measurements of several different physical quantities," Nucl. Instrum. Meth. A **500**, 391 (2003).

[21] R. Nisius, "BLUE: a ROOT class to combine a number of correlated estimates of one or more observables using the Best Linear Unbiased Estimate method," http://blue.hepforge.org

List of Tables

List of Figures